Brain, Behavior, & Immunity - Health 32 (2023) 100669

Contents lists available at ScienceDirect

Brain, Behavior, & Immunity - Health

journal homepage: www.editorialmanager.com/bbih/default.aspx

In utero and post-natal opioid exposure followed by mild traumatic brain injury contributes to cortical neuroinflammation, mitochondrial dysfunction, and behavioral deficits in juvenile rats

Austin M. Gowen [a], Jina Yi [a], Kelly Stauch [b], Luke Miles [a,c], Sanjay Srinivasan [a,d], Katherine Odegaard [e], Gurudutt Pendyala [a,f,g,h], Sowmya V. Yelamanchili [a,f,h,*]

[a] Department of Anesthesiology, University of Nebraska Medical Center, Omaha, NE, USA
[b] Department of Neurological Sciences, University of Nebraska Medical Center, Omaha, NE, USA
[c] Department of Psychological and Brain Sciences, Dartmouth College, Hanover, NH, USA
[d] Department of Biological Sciences, University of Nebraska at Omaha, Omaha, NE, USA
[e] Department of Biological Sciences, Florida State University, Tallahassee, FL, USA
[f] Department of Genetics, Cell Biology and Anatomy, UNMC, Omaha, NE, 68198, USA
[g] Child Health Research Institute, Omaha, NE, 68198, USA
[h] National Strategic Research Institute, UNMC, Omaha, NE, USA

ARTICLE INFO

Keywords:
Opioid
Neonatal opioid withdrawal syndrome
Minor traumatic brain injury
Cortex
Synaptosome
Mitochondria
Neuroinflammation

ABSTRACT

Maternal opioid use poses a significant health concern not just to the expectant mother but also to the fetus. Notably, increasing numbers of children born suffering from neonatal opioid withdrawal syndrome (NOWS) further compounds the crisis. While epidemiological research has shown the heightened risk factors associated with NOWS, little research has investigated what molecular mechanisms underly the vulnerabilities these children carry throughout development and into later life. To understand the implications of *in utero* and post-natal opioid exposure on the developing brain, we sought to assess the response to one of the most common pediatric injuries: minor traumatic brain injury (mTBI). Using a rat model of *in utero* and post-natal oxycodone (IUO) exposure and a low force weight drop model of mTBI, we show that not only neonatal opioid exposure significantly affects neuroinflammation, brain metabolites, synaptic proteome, mitochondrial function, and altered behavior in juvenile rats, but also, in conjunction with mTBI these aberrations are further exacerbated. Specifically, we observed long term metabolic dysregulation, neuroinflammation, alterations in synaptic mitochondria, and impaired behavior were impacted severely by mTBI. Our research highlights the specific vulnerability caused by IUO exposure to a secondary stressor such as later life brain injury. In summary, we present a comprehensive study to highlight the damaging effects of prenatal opioid abuse in conjunction with mild brain injury on the developing brain.

1. Introduction

The ongoing opioid epidemic has seen record numbers of children born suffering from neonatal opioid withdrawal syndrome (NOWS) caused by *in utero* opioid exposure (Kuehn, 2018). The ability for opioids to pass both the placental barrier and blood-brain barrier (BBB) makes them particularly impactful neurological teratogens (Yazdy et al., 2015; Larson et al., 2019; Little et al., 2021). First line therapeutic interventions for NOWS relies on a methadone weaning protocol to avoid withdrawal related complications, further extending the duration children are exposed to opioids (Hall et al., 2015). *In utero* opioid exposure causes many neuropathophysiological outcomes including cortical thinning, increased basal neuroinflammation, attenuated myelination, motor deficits, behavioral issues, and cognitive impairment (Larson et al., 2019; Little et al., 2021; Yeoh et al., 2019; Hartwell et al., 2020; Vasan et al., 2021). Significant advances have been made in establishing the negative molecular and physiological sequelae associated with *in utero* opioid exposure, however, to date there has been few reports understanding how these changes would impact later life development. Broadly, gestational insults as a whole have been well

* Corresponding author. Department of Anesthesiology, University of Nebraska Medical Center, Omaha, NE, USA.
E-mail address: syelamanchili@unmc.edu (S.V. Yelamanchili).

https://doi.org/10.1016/j.bbih.2023.100669
Received 21 July 2023; Accepted 22 July 2023
Available online 28 July 2023

understood to induce later life vulnerability to injury and disease, and many studies have also observed these epidemiological effects in children suffering from NOWS (Larson et al., 2019; Yeoh et al., 2019; Liu et al., 2019; Oei et al., 2017). Interestingly, recent data shows that children who suffered from NOWS have a significantly increased rate of emergency department (ED) visits throughout childhood (Liu et al., 2019). This makes *in utero* opioid exposure a marked risk factor for later life injury and disease in a potentially vulnerable population; in fact, falls are the most common non-fatal injury for ED admittance in children and are the primary cause of pediatric mild-traumatic brain injury (mTBI) (Taylor et al., 2017). Given the well reported association of NOWS with motor-control deficits and motor cortex thinning persistent through peri-adolescence (Larson et al., 2019; Hartwell et al., 2020) there is an urgent need to understand if this population is more vulnerable to one of the most prevalent pediatric injuries: mTBI (Yeoh et al., 2019).

mTBI is one of the most common injuries with a 2020 report showing that 8.3% of children were diagnosed with at least one concussion before reaching 18 years old, and self-reported numbers being significantly higher (Concussions and Brain Injuries in, 2021). The primary cause of mTBI in children is from slips, falls, and accidents during play (Araki et al., 2017). The acute sequelae of mTBI overlap significantly with *in utero* opioid exposure associated pathophysiology such as increased inflammation, myelin disruption, and cognitive deficits. However, mTBI associated patient-perceived symptoms can be recoverable in as short of a time frame as 15 min to 2 weeks in most cases (Carroll et al., 2004). Despite this a significant minority of mTBI sufferers have longitudinal symptoms that impose serious deficits including fatigue, pain, cognitive deficits, mood disorders, and accelerated neurodegenerative disease progression (Li et al., 2016; Perry et al., 2016; Johnson et al., 2013; Tweedie et al., 2020; Arciniegas and Wortzel, 2014; Calvillo and Irimia, 2020). What is poorly understood is why some individuals develop these negative symptoms post-mTBI while others recover normally. Currently, the dominant theory is that individuals with poor outcomes have an innate or induced susceptibility to neurotrauma due to genetic or environmental risk factors, yet what these risk factors are remains largely unknown (Cherry et al., 2018; Asken et al., 2016; Rickards et al., 2022; Caplain et al., 2017). Considering the impact of *in utero* opioids on increased risk-factor for ED admissions and impaired motor function, it is possible that early exposure during a critical developmental period causes impaired ability to recover from mTBI.

In the current study, we utilized a previously established regimen to mimic *in utero* and post-natal oxycodone exposure (IUO) in a rat model, combined with a low-force closed-head weight drop model of mTBI to demonstrate a recoverable brain injury that could be caused by a slip or fall which make up the majority of juvenile mTBI (Taylor et al., 2017). Utilizing a closed head weight drop model is ideal for investigating head injuries similar to those seen in the pediatric population because it mimics both the contusion injury at the site of injury as well as the rotational acceleration associated injury (Shultz et al., 2017). Applying both molecular and behavioral tools, for the first time, we demonstrate that IUO exposure creates a susceptible environment in the brain, that when challenged with a mild stressor such as mTBI, results in significant damage to later life development. These data shed light on novel mechanisms that warrants for not only patient and provider investigation into brain trauma, but also, provides new directions to potentially treat the growing NOWS epidemic.

2. Methods

2.1. Animals

Male and female Long Evans 006 rats were obtained from Charles River Laboratories Inc. (Wilmington, MA, USA) and condition housed in a 12 h light–dark cycle and fed ad libitum. Equal ratio of sex distribution (n = 3) was used for all molecular experiments to accurately represent the population distribution. Sex differences were statistically assessed in all experiments, however n = 3 provides insufficient power to ascertain sex differences. For all experiments 1 male and 1 female animal from N = 3 biological dams were used. Pups from 14 saline gavaged dams and 16 oxycodone gavaged dams were used in these works. Animals were assigned randomly to various experimental groups within litters by Excel random number generation blocking. Power analysis was performed using previously published works as a baseline reference to determine sample sizes (Odegaard et al., 2020a, 2020b; Shahjin et al., 2019). All procedures and protocols were approved by the Institutional Animal Care and Use Committee of the University of Nebraska Medical Center and conducted in accordance with the National Institutes of Health Guide for the Care and Use of Laboratory Animals.

2.2. In utero oxycodone treatment

The development of the IUO treatment paradigm was adapted from previously published studies (Odegaard et al., 2020a, 2020b; Shahjin et al., 2019). Nulliparous female (70–80 days of age) Long Evans rats were treated with oxycodone HCl (Sigma Aldrich, St. Louis, MO, USA) dissolved in saline via oral gavage, a graphical timeline is included in the supplement (Supplementary Fig. 1). An ascending dosing procedure was used wherein doses of 10 mg/kg/day oxy were orally gavaged for 5 days. After five days a final dose of 15 mg/kg/day was administered, after which females were mated with proven male breeders, and the treatment regimen continued throughout mating, gestation, and parturition until weaning at post-natal day (P) 21. Pups are removed at P21 and allowed to recover from opioid exposure for 7 days. Because the half-life of oxy is relatively short and drug distribution can be altered by pregnancy, dams were monitored daily for signs of opiate withdrawal, such as weight loss, diarrhea, and irritability throughout gestation.

2.3. Phenotypic measurements

Body weight and head size diameter, as measured from the front of each ear, were obtained from saline and IUO conditions at P28 prior to injury. After injury righting reflex, or time to right (TTR) was recorded as the time from impact until a supinated animal placed pronates and mobilizes all four limbs supporting its own weight. For all animals time was kept ensuring that no more than 5 s passed from removal from anesthesia to mTBI induction.

2.4. mTBI procedures

This procedure was adapted from Mychasiuk et al., 2014) (Mychasiuk et al., 2014). At P28 rats were placed in a pre-primed isoflurane chamber with 5% isoflurane in 100% oxygen for 45 s to induce anesthesia. Animals were removed from the chamber and subjected to a toe-pinch to assess sufficient plane of anesthesia. Animals were then placed, pronated, on a scored tin-foil platform 15 cm above a foam landing pad. A guide tube was centered above the mid-line of the subjects' head. A 100-mg weight was locked at the 500-cm height with a 505-cm line attached; the weight was released and allowed to free-fall and impact the subject. Subjects broke through the scored tin-foil base and were allowed to freely rotate post-impact to land supinated on the foam landing pad. Animals were subcutaneously administered 1 mg/kg of bupivacaine to the site of impact and placed, supinated, in a cage and observed until normal movement was observed. No mortality or signs of complication were observed in any subjects post-mTBI. No skull fractures were observed post-mortem, but some bleeding was observed (Supplementary Fig. 2) Sham conditions were identically anesthetized, placed on the tin-foil platform, and given 1 mg/kg bupivacaine, however, no mTBI or rotational movement was suffered. The four conditions seen in the study are *in utero* saline exposure with sham (Sal + Sham), *in utero* saline exposure with mTBI (Sal + mTBI), *in utero* oxycodone exposure with sham (IUO + Sham), and *in utero* oxycodone exposure

with mTBI (IUO + mTBI).

2.5. RNA isolation and qRT-PCR

Total RNA from cortex tissue was isolated from the randomly selected male or female pups of each treatment condition at DPI 2, 6, 10, and 38–40 using the Direct-Zol RNA kit (Zymo Research, CA, USA). A custom TaqMan probe plate was purchased from Applied Biosystems designed for mTBI and inflammation associated genes (Supplementary Table 1). Analysis by real-time PCR (rt-PCR) was performed, and the delta-delta Ct method was used to calculate fold change and statistical significance as previously described (Odegaard et al., 2020a).

2.6. Immunohistochemical (IHC) analysis

Rat brains were collected after perfusion with sterile 1× PBS followed by 4% PFA. Brains were placed in cooled 4% PFA overnight at 4 °C. Following this, brains were cryoprotected by resting in a solution of 20% sucrose for 24 h followed by a 30% sucrose solution for 24 h at 4 °C. Following sucrose preparation tissues were snap frozen in Optical Cutting Temperature Compound (OCT) molds via immersion in a pre-cooled −80 °C 2-methylbutane bath. Frozen tissues were stored at −80 °C until cryosectioning. Sections were cut at −20 °C in 10 μm thick sections at interaural 6.48 mm and bregma −2.52 axes as described by Paxinos and Watson's rat brain atlas to include both the site of direct injury as well as the primary and secondary motor cortex. Tissues were warmed to 37 °C for 10 min then washed in 1× PBS three times before being permeabilized for 15 min in 0.3% Triton. Permeabilized tissue was blocked using 3% normal goat serum and 3% FBS before incubation at 4 °C overnight in primary antibody (Supplementary Table 2). Sections were then washed in PBS three times before 1-h incubation with appropriate secondary antibody and DAPI for nuclear staining. Sections were mounted using Prolong Gold Antifade reagent. Sections were imaged using EVOS M5000 (Thermo Fisher) microscope with DAPI (357/447 nm), GFP (470/525 nm), and Texas Red (585/524) fluorescent light cubes. Microglia were labeled using primary Iba1/Aif1 and secondary Alexa Fluor 488 secondary (Supplementary Table 2). Quantification images were captured at the apical cortex using 10× magnification, and representative images were taken using a 40× magnification. Cell quantification was performed using FIJI (Schindelin et al., 2012) by converting 10× IHC captured images to 8-bit then threshold gating using Sal + Sham controls to assess number of cells and relative size of microglia for all conditions.

2.7. ^{1}H-MRS acquisition

P30 pups were used for *in vivo* localized ^{1}H-MRS imaging of the cortex similarly to previously published works in the hippocampus (Odegaard et al., 2020b). Animals were anesthetized using 1–1.5% isoflurane in 100% oxygen and maintained 40–80 breaths/minute. MRI and ^{1}H-MRS data were obtained using a Bruker® Biospin 7 T/21 cm small animal scanner (Bruker, Billerica, MA), operating at 300.41 MHz, using a laboratory-built 22 mm diameter quadrature birdcage volume coil. All first- and second-order shim terms were first automatically adjusted in the volume-of-interest (VOI) using MAPSHIM® (Bruker, Billerica, MA), with a final shim performed manually to achieve a water line width of 10–15 Hz. The water signal was suppressed by variable power radiofrequency pulses with optimized relaxation delays (VAPOR). MR images were acquired for anatomical reference using a multi-slice rapid acquisition with relaxation enhancement (RARE) sequence (Effective echo time (TE) = 36 ms, Rare Factor = 8, repetition time (TR) = 4200 ms, Number of Averages (NA) = 2, Scan Time = 3 m 21 s; FOV = 20 × 20 mm^2, Matrix Size = 256 × 256, Spatial Resolution = 0.078125 × 0.078125 mm^2, Number of Slices = 29, Slice Thickness = 0.5 mm). ^{1}H-MRS data sets were obtained using semiLASER localization with timing parameters (TE/TR = 40/4000 ms, 576 averages, 2048 points) from a 2 × 5.187 × 1.557 mm3 (16.15 μL) VOI located in the mid-cortex. Pulse types and specifications: Excitation: hermite 90, duration = 0.7 ms, bandwidth = 5400 Hz; 1st and 2nd Refocusing: hyperbolic secant, duration = 4 ms, bandwidth = 9484.5 Hz. The acquisition time was 38:24 min per data set. All pulses were applied with a frequency offset of −600 Hz to center the pulse bandwidth between Creatine (CRE) and N-Acetyl Aspartate (NAA). For the water suppression module, the spoiler strength matrix was calculated automatically. Spoiler strength was 35%; spoiler duration was 1.5 ms. For each experiment, one data set was acquired without water suppression to be used as the water concentration reference during quantitation. Unsuppressed water spectra were obtained with identical metabolite spectra parameters except for the following: TR = 10,000 ms, NA = 1, and Receiver Gain = 64. One 64 average (for quality assessment) plus four 128-average data sets were acquired for metabolite measurements using a combination of VAPOR scheme for water suppression. Model parameters and constraints for quantification were generated using spectra from phantoms (n = 14) for the following metabolites: Alanine (ALA), Aspartate (ASP), Gamma-Aminobutyric acid (GABA), Glucose (GLC), Glutamine (GLN), Glutamate (GLU), Glycine (GLY), Lactate (LAC), Myo-inositol (MYO), Phosphorylcholine (PC), Taurine (TAU), total choline (tCHO), CRE, and NAA. Phantoms of each metabolite were prepared in pH 7.5 phosphate buffer (100 mM) and contained 3-(trimethylsilyl)-1-propane-sulfonic acid and sodium formate as chemical shift and phasing references. Spectra for each metabolite at known concentrations were acquired using semiLASER sequences at 40 ms TE, maintaining the phantom at 38 °C with a circulating water jacket during spectral acquisition. The set of metabolite spectra formed a metabolite basis set, which was used as prior knowledge during quantification. In all conditions, n = 6 except for IUO + Sham (n = 5) where one female animal was excluded for imaging complications.

2.8. Purified synaptosome isolation

To investigate the effects of *in utero* and postnatal oxy exposure on synaptic transmission, we isolated purified synaptosomes (SYP) following the protocol designed by Ahmed, Holt, Riedel, and Jahn (Araki et al., 2017) with minor modifications. 500 mg of cortical tissue from each condition (n = 6) was homogenized in 9 mL of ice-cold homogenization buffer (320 mM sucrose, 4 mM HEPES, protease inhibitor tablet) using a Wheaton Overhead Stirrer with ten strokes at 2 k–3k RPM. The homogenized mixture was centrifuged at 1000 × *g* for 10 min at 4 °C, and the pellet (P1; cell fragments and nuclei) was discarded. The supernatant was centrifuged at 12,000 × *g* for 20 min at 4 °C. The pellet (P2; crude synaptosomes) was washed carefully in 1 mL of homogenization buffer. Suspended crude synaptosomes were layered on top of a sucrose gradient (1.20 M, 0.80 M, and 0.60 M) and spun in a SW41 Ti Rotor (Beckman Coulter, Brea, CA, USA) at 145,000 × *g* for 40 min at 4 °C. The synaptosomal band was collected at the 0.80 M and 1.20 M interface. The collected band was resuspended with 9 mL of homogenization buffer and spun again using the SW41 Ti Rotor at 145,000 × *g* for 40 min at 4 °C. This pellet was resuspended in 200–300 μL of PBS + protease inhibitor (Roche Diagnostics) depending on the size of the pellet garnering our purified synaptosome samples.

2.9. Mass spectrometry

Mass spectrometry was performed using previously published methodologies (Nguyen et al., 2022). Briefly, 100 μg of protein per purified SYP sample from six biological replicates per condition was taken, and detergent was removed by chloroform/methanol extraction. With 100 mM ammonium bicarbonate, the protein pellet was resuspended followed by digestion with MS-grade trypsin (Thermo Fisher) at 37 °C overnight. PepClean C18 spin columns (Thermo Scientific) were used to clean peptides. Cleaned peptides were re-suspended in 2% acetonitrile (ACN) and 0.1% formic acid (FA), and 500 ng of each

sample was loaded onto trap column Acclaim PepMap100, 75 μm × 2 cm C18 LC Columns (Thermo Scientific) at a flow rate of 4 μL/min. Samples were then separated with a Thermo RSLC Ultimate 3000 (Thermo Scientific) on a Thermo Easy-Spray PepMap RSLC C18, 75 μm × 50 cm C-18 2 μm column (Thermo Scientific) with a step gradient of 4–25% solvent B (0.1% FA in 80% ACN) from 10 to 130 min and 25–45% solvent B for 130–145 min at 300 nL/min and 50 °C with a 180-min total run time. Following separation, the Thermo Orbitrap Fusion Lumos Tribrid (Thermo Scientific) mass spectrometer, in a data-dependent acquisition mode, was used to analyze the eluted peptides. All samples were batched and randomized for all runs. An MS scan (from m/z 350–1800) was acquired in the Orbitrap with a resolution of 120,000. The AGC target for MS1 was set as 4 × 105 and ion filling time set as 100 ms. To isolate the most intense ions a charge state of 2–6, a 3 s cycle was performed followed by fragmentation using HCD fragmentation with 40% normalized collision energy and detected at a mass resolution of 30,000 at 200 m/z. The AGC target for MS/MS was set as 5 × 104 and ion filling time set at 60 ms; dynamic exclusion was set for 30 s with a 10-ppm mass window. For identification of proteins a search was conducted where the MS/MS data were viewed against the Swiss–Prot *Rattus norvegicus* protein database downloaded in May 2019, using the in-house mascot 2.6.2 (Matrix Science, Canton, MA, USA) search engine. The search criteria consisted of full tryptic peptides with a maximum of two missed cleavage sites. The variable modifications included acetylation of protein N-terminus and oxidized methionine. The fixed modification was carbamidomethylation of cysteine. Additional parameters set include the precursor mass tolerance threshold, which was set at 10 ppm, and the maximum fragment mass error which was set at 0.02 Da. A false discovery rate (FDR) of ≤1% was used to determine the significant threshold of the ion score. Progenesis QI proteomics 4.1 (Nonlinear Dynamics, Milford, MA, USA) was then utilized to perform qualitative analysis.

2.10. Bioinformatics

Identified proteins were pruned for those with 2 or more unique peptides. Proteins were considered differentially expressed if the FDR-corrected p-value was ≤0.05 and displayed a fold change ≥1.5. Further exclusion criteria were placed to reduce the number of significant upregulated hits in the IUO + Sham and IUO + mTBI conditions by only including proteins with a fold change ≥1.5 as compared to ACTB. Venn diagram was generated using bioinformatics. psb.ugent.be/webtools/Venn/online resource. Heatmap was generated using the top expressed mitochondrial proteins shared between IUO + Sham and IUO + mTBI conditions in Graph Pad Prism software (La Jolla, CA, USA). Cytoscape plugin ClueGO was used to perform gene ontology (GO) analysis of biological processes on significantly differentially expressed proteins (Shannon et al., 2003); criteria placed were: *Rattus norvegicus*, all experimental, GO term fusion, and pV ≤ .05. Further, enriched disease-associated pathways were identified using the Ingenuity Pathway Analysis (IPA) software (Ingenuity® Systems, Redwood City, CA, USA). Canonical pathway analysis in IPA was performed by comparing the differentially expressed proteins against known canonical pathways (signaling and metabolic) within the IPA database.

2.11. Immunoblotting

15μg of protein as determined by Pierce bicinchoninic acid assay (Thermo Fisher Scientific, Waltham, MA, USA) from each animal were loaded into 4–12% Bis-Tris wells (Invitrogen, Waltham, MA, USA) under reducing conditions, followed by transfer to a nitrocellulose membrane using iBlot2 (Invitrogen). Ponceau S stain (Thermo Fisher Scientific) was used on the nitrocellulose membrane for equal protein loading detection and quantification. SuperBlock was used to block nonspecific antibody binding (Thermo Fisher Scientific, Waltham, MA, USA). After blocking, membranes were incubated overnight at 4 °C with a primary antibody (Supplementary Table 2). Primary and secondary antibody dilutions were done according to the manufacturer's suggestion and are shown in Supplementary Table 2. Blots were developed using Azure cSeries Imager (Azure Biosystems, Dublin, CA, USA) with SuperSignal West Pico Chemiluminescent Substrate (Thermo Scientific).

2.12. Isolation of synaptic and non-synaptic mitochondria

Synaptic mitochondria were isolated from P30 rats 2 days post-injury using modifications to a method described previously (Huang et al., 2014). Following decapitation, brains were rapidly removed, micro-dissected and placed in ice-cold isolation medium (IM) containing 225 mM sucrose, 75 mM mannitol, 1 mM EGTA, 5 mM HEPES, and cOmplete Mini, EDTA-free protease inhibitor cocktail (Roche Diagnostics) adjusted to pH 7.4. All homogenization and centrifugation steps were carried out on ice and at 4 °C, respectively. Brains were minced and homogenized with 35 strokes in a Dounce homogenizer. The homogenate was then centrifuged at 1300×*g* for 3 min. Supernatant was collected and the pellet was resuspended in IM and centrifuged again at 1300×*g* for 3 min. The pooled supernatants were centrifuged at 21,000×*g* for 10 min. This pellet was then resuspended in 15% Percoll and layered on top of a 24% and 40% Percoll gradient (prepared from 100% Percoll solution containing 225 mM sucrose, 75 mM mannitol, 1 mM EGTA, and 5 mM HEPES adjusted to pH 7.4 with HCl). Following centrifugation for 8 min at 30,700×*g* the banding near the interface of the upper two layers of the gradient, containing synaptosomes, was collected and diluted in IM. This synaptosomal fraction was then transferred to a nitrogen cavitation vessel (Parr Instrument Company) where the pressure was equilibrated to 1000 psi for 30 min followed by depressurization to ATM pressure, which released synaptic mitochondria. This suspension was then added to the top of 24% Percoll and centrifuged for an additional 10 min at 30,700×*g*. The pellet containing the synaptic mitochondria was resuspended in IM and centrifuged at 16,700×*g* for 10 min. Finally, the pellet was resuspended in IM with fatty acid free BSA followed by centrifugation at 6900×*g* for 10 min. This final pellet containing (w/v) SDS and 0.1 M DTT adjusted to pH 7.6. Lysates were incubated at 95 °C for 5 min then briefly sonicated. Protein concentrations were determined using a Pierce 660 nm Protein Assay.

2.13. Seahorse electron flow analysis of synaptic and non-synaptic mitochondria

The Seahorse XF24 Flux Analyzer (Seahorse) was equilibrated to 37 °C overnight and a modified protocol was used based on previous work in mouse liver mitochondria. Equal numbers of isolated synaptic and non-synaptic (10 μg as determined by Pierce 660 nm Protein Assay) were plated in V7-PS XF24 cell culture microplates in a volume of 50 μL mitochondrial assay solution (MAS) containing 70 mM sucrose, 220 mM mannitol, 10 mM KH_2PO_4, 5 mM $MgCl_2$, 2 mM HEPES, 1 mM EGTA and 0.2% fatty-acid free BSA with 10 mM pyruvate, 2 mM malate, and 4 μM carbonyl cyanide-*p*-trifluoromethoxyphenylhydrazone (FCCP). After centrifugation for 15 min at 2000×*g* to attach mitochondria, 450 μL of MAS (containing substrate) was added to each well, and the plate was incubated at 37 °C for 8 min to equilibrate temperature. The final concentrations of additions to the wells were 4 mM ADP, 2.5 μg/mL oligomycin, 4 μM FCCP, and 4 μM antimycin A for the coupling assay and 2 μM rotenone, 10 mM succinate, 4 μM antimycin A, and 10 mM ascorbate with 100 μM tetramethylphenylenediamine (ASC/TMPD) for the electron flow assay. The electron flow assays were run in 6 technical replicate wells for each independent biological replicate. Technical replicates that had reagent injection issues according to seahorse software analysis were excluded. XF24 data was calculated using the algorithm previously described and used by the Seahorse software package (Rogers et al., 2011). Statistical analysis was conducted in PRISM (GraphPad Software) using one-way ANOVA and post-test with Tukey's multiple comparison tests.

2.14. Rotarod

P61-64 animals were assessed for motor function and balance using the Rotarod (Panlab, Model LE8305 76–0771; Barcelona, Spain). A central rod with a diameter of 60 mm made of Perspex and knurled to provide adequate grip is divided into 5 lanes. Animals were placed on the rod within a lane 215 mm above a trip box at a starting speed of 4 rotations per minute (RPM). The start of time recording began an acceleration protocol by which the rod would increase its RPM by .12 rotations per second to a maximum of 40 rotations over a 300 s period. Animals underwent 6 independent trials with 20 min between each trial. The first three trials were considered training trials, while the last three trials were considered performance trials. Rats were placed on the rotarod for 10s at 4 RPM, and then latency to fall was measured for each animal after acceleration protocol began. Rats were considered to fall if they fell from the rod, turned around, or clung to the rod for two full rotations. All assessments were conducted within the first 6 h of the animal facility light-cycle.

2.15. Marble burying

P61-64 animals were assessed for activity and anxiety using marble burying assessment as described in previously published works (Odegaard et al., 2020a). A rat cage (929 cm^2, 43.18 × 21.59 × 20.32 cm) containing an even 5 cm layer of ¼-inch corncob bedding (Envigo #7097), and 20 standard glass marbles (15 mm diameter, 5.2 g) were lightly placed in a 5 × 4 arrangement on top of the bedding. The subject was placed into the cage, and the cage was covered for 30 min. The animal was removed, and the marbles were imaged and scored by a scorer blinded to conditions. A marble was considered buried if more than 70% of the marble was under the bedding. All assessments were conducted within the first 6 h of the animal facility light-cycle.

2.16. Social preference and social novelty

Both social novelty and social preference were carried out in P65 animals using an in-house built chamber as described in previously published works (Odegaard et al., 2020a). Briefly, a 90 × 40 × 40 cm acrylic chamber was divided into three 30 × 40 × 40 cm compartments. The left and right compartments contained 15 × 15 × 40 cm perforated isolation cubes. Perforations were spaced 1 cm apart along the entirety of both isolation cubes to allow for scenting and touching but not entrance.

To evaluate social novelty, a naive animal of the same sex and of similar age and size was placed into the left isolation cube. A cagemate of the test animal's housing cage was placed into the right isolation cube. The test animal was placed into the central chamber. For assessing social preference, a new naive rat (not used in social novelty) was placed into the left isolation cube, a rubber toy in the right isolation cube, and the test animal into the central chamber. After 5 min of acclimation, the two doors were lifted and the test animal was allowed to freely explore the entirety of the social chamber for 15 min. Animals were then returned to their housing cages, and the social chamber was cleaned and sterilized.

Scoring for both social tests consisted of the time the animal spent in each chamber, the number of entries into each chamber, and the number of active contacts toward one of the isolation cubes. Entry into a chamber was scored if an animal's head and all four paws were within the compartment. An active contact was defined as any attempt to sniff, paw, scratch, touch, or stretch toward any of the isolation cubes when inside the compartment containing an isolation cube. Testing was recorded, and recordings were scored manually by scorers blinded to the conditions. All assessments were conducted within the first 6 h of the animal facility light-cycle.

2.17. Hot plate nociception testing

An animal was placed on an Incremental Hot Plate set at a starting temperature of 25 °C (IITC Life Science, Irving, CA, U.S.A.). Temperature increased by 5 °C per minute with maximum temperature of 50 °C. During testing animals were constantly monitored by an attendant. When the animal licked its back paw, a standardized behavior to avoid heat, the test was stopped. Duration and intensity of heat was recorded using software provided by IITC Life Science. The testing plate was sanitized between each run to prevent eliminate scent-related confounds. All assessments were conducted within the first 6 h of the animal facility light-cycle.

2.18. Maternal pup retrieval

A total of n = 6 dams with litters between 9 and 12 pups per condition were assessed for maternal behavior at 3 days post-birth. Dams were taken to the behavioral room at the beginning of their light cycle. A 1 h acclimation period was allowed. The dam was allowed to voluntarily end nursing and was then removed from the home chamber temporarily. Three randomly selected pups were moved to three corners of the cage furthest from the central nursing nest. Dam was returned to the center of the home cage and recording begins. Time till first retrieval, second retrieval, third retrieval, and crouched nursing was recorded over a duration of 10 min. If dams failed to initiate nursing within 10 min their recording was noted at 600 s. Home cage was returned to animal room and left undisturbed. Pups in litters used for pup retrieval were not used in any further behavioral assessment.

2.19. Statistical analyses

Data were analyzed for outliers using standard outlier tests in GraphPad Prism (version 9.3.1) finding that all data was normally distributed. Significance was determined using appropriate statistical testing outlined within figure legends for specific comparisons made followed by Tukey's or Dunnett's multiple comparison correct where appropriate with a minimum criterion for significance of $p \leq 0.05$. All data are presented as mean ± SEM with individual data points. Fig. 1a and b data were analyzed using Welch's unpaired *t*-test to compare between two conditions to compare populations with unequal sample size. In Figs. 1c, 6a-c, 7a-c, and 9a-c when comparing between four conditions Sal + Sham, Sal + mTBI, IUO + Sham, and IUO + mTBI one-way ANOVA was performed with Tukey's multiple comparison correction if the same control animals were used between comparisons. In Fig. 2a–c, 3c, 3d, 4, 8a-d, and 9 d two way ANOVA was performed when comparing multiple variables between the four conditions with Tukey's multiple comparison correction when the same control animals were used between comparisons. Results were visualized using GraphPad Prism (version 9.3.1).

2.20. Data availability

The derived data supporting the findings of this manuscript are included within the manuscript or in the supplementary files. Further data inquiries can be directed to the corresponding author.

3. Results

3.1. IUO induces disparities to development and righting reflex Post-mTBI

IUO exposure has been reported to affect physiological development in murine and rat models, including weight, head size, and BMI (Odegaard et al., 2020a, 2021; Jantzie et al., 2020a; Newville et al., 2020; Merhar et al., 2021; Boggess and Risher, 2022; Bailey et al., 2022). To assess the effect of the IUO exposure on physiological development, we measured the weight and head circumference as previously described

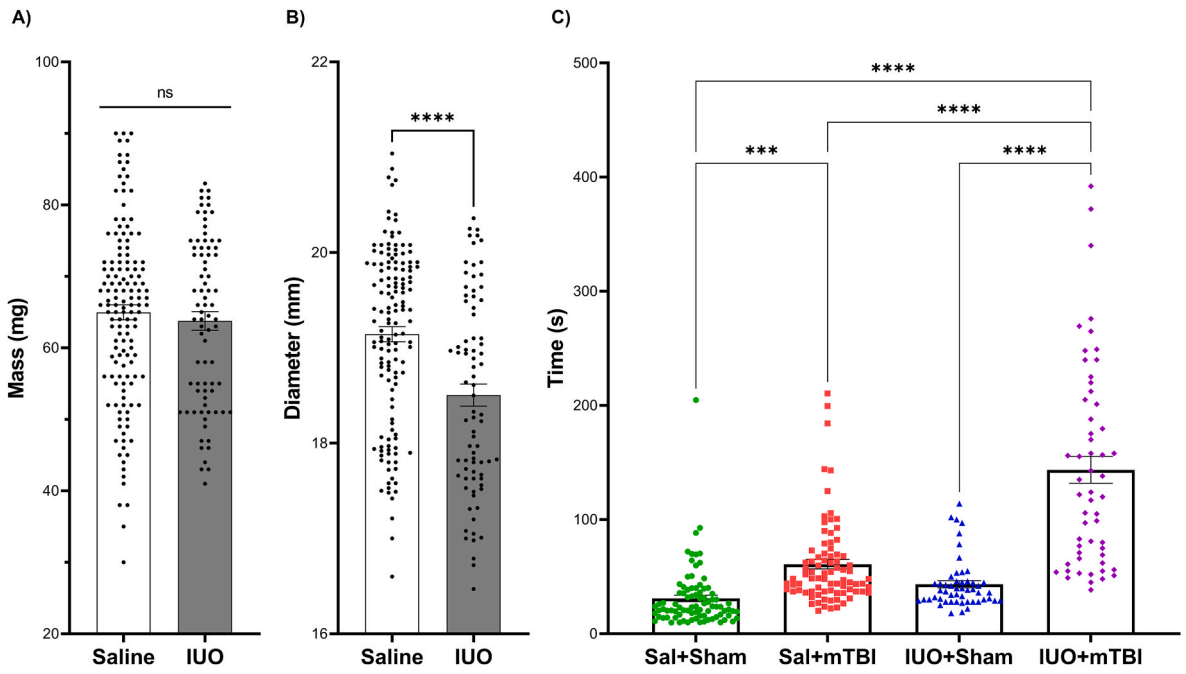

Fig. 1. IUO exposure causes pathophysiological head diameter and righting reflex in response to mTBI. At post-natal day 28 *in utero* saline (Saline) and oxycodone (IUO) exposed animals were subjected to Sham or mTBI procedures and measured for weight, head diameter, and righting reflex. **(A)** IUO exposure does not significantly affect animal weight at P28 ($p \geq 0.48$) but significantly decreases **(B)** head diameter. Data is represented as Mean ± SEM, n = 141 for Saline and n = 80 for IUO; ****$p < 0.0001$. Welch's unpaired *t*-test was performed. **(C)** Post-anesthesia either Sham or mTBI procedure animals were assessed for their time-to-right (TTR). Sal + mTBI groups showed a significantly increased TTR when compared to Sal + Sham conditions ($p \leq 0.004$); IUO + mTBI conditions had a significantly increased TTR as compared to Sal + Sham ($p \leq 0.0001$), Sal + mTBI ($p \leq 0.0001$), and IUO + Sham ($p \leq 0.0001$). Data are represented as Mean ± SEM; n = 86 for Sal + Sham, n = 82 for Sal + mTBI, n = 52 for IUO + Sham and n = 56 for IUO + mTBI; *$p \leq 0.05$, **$p \leq 0.001$, ***$p \leq 0.005$, ****$p \leq 0.0001$. One-way ANOVA with Tukey's multiple comparison test was performed.

(Odegaard et al., 2020c). IUO and saline exposed conditions were measured at post-natal day (P) 28, an age that mimics early childhood in humans and corresponds not only to a highly active stage for neurological development but also a vulnerable age for mTBI (Andersen, 2003). At P28, IUO exposed conditions did not show significant alterations in weights as compared to the saline condition (Fig. 1a), however, displayed significantly decreased head diameter (Fig. 1b). Next, the saline and IUO rats underwent mTBI procedure and righting reflexes or time-to-right (TTR) was calculated to inform on the severity of injury as a measure of the rats' ability to regain normal motor function. TTR as defined by time it takes a supinated rat to awaken from anesthesia and mobilize all four limbs supporting its own weight after mTBI or sham induction. Within the saline conditions, a significant increase ($p \leq 0.004$) in TTR was observed in animals that underwent mTBI (Sal + mTBI) when compared to animals that underwent the sham procedure (Sal + Sham) (Fig. 1c). Within the IUO conditions, animals that underwent mTBI (IUO + mTBI) displayed significant increase in TTR when compared to IUO + Sham ($p \leq 0.0001$) but also when compared across other saline conditions, Sal + Sham ($p \leq 0.0001$) and Sal + mTBI ($p \leq 0.0001$). On the other hand, no significant differences were seen between the saline and IUO conditions that underwent just the sham procedure. Further, the data also suggests that the combination of IUO + mTBI has a greater impact on TTR when compared to IUO exposure or mTBI alone with a 3.31-fold and 2.35-fold increase in TTR, respectively.

3.2. Assessment of cortical neuroinflammatory and classical biomarkers Post-mTBI

To understand the effects of IUO in the brain post-TBI, we assessed the expression of several well reported marker genes associated with mTBI induced inflammation across days post injury (DPI) 2 and 10 (McDonald et al., 2021). At DPI 2, qRT-PCR analysis revealed a significant increase in both the inflammatory (*Aif1, Il1β, Il6, and Tnfα*, Fig. 2a) as well in classical mTBI biomarkers (*Bdnf, Mapt, Mbp, Nefl, and S100β*, Fig. 2b) in the Sal + mTBI conditions when compared to Sham controls (McDonald et al., 2021). Further, no significant upregulation in the expression of inflammatory genes was observed at DPI 10 in Sal + mTBI conditions, apart from one gene, *Nefl,* that showed increased expression (Fig. 2b). On the other hand, the IUO conditions (IUO + Sham and IUO + mTBI) displayed significant upregulation of inflammatory genes: *Cxcl1, Il6, and Tnfα*, across all DPI timepoints (Fig. 2c & e). Additionally, classical mTBI biomarker genes (*Bdnf, Mapt, Nefl, and S100β*) were significantly upregulated across all DPI timepoints (Fig. 2d & f). However, no significant differences were seen between IUO + mTBI conditions when compared to IUO + Sham. Additional assessment of these genetic markers of inflammation and mTBI was performed again at DPI 38–40, and found *Aif1* and *Bdnf* to still be significantly elevated in both IUO + Sham and IUO + mTBI conditions when compared to Sal + Sham (Supplementary Fig. 3). Next, we performed immunohistochemistry (IHC) to investigate inflammatory cells of the brain, microglia, at the superior site of the cortex closest to the weight drop impact. IHC results show no significant changes in microglia count in the Sal + mTBI conditions as compared to the Sal + Sham but a trending increase (not significant) at DPI 2 and 10 (Fig. 3). However, in the IUO + mTBI we see significant increase in microglia numbers and size at DPI 2 and 10 suggesting an exacerbated response after acute injury with an impaired ability to return to baseline post 10 days mTBI (Fig. 3). The increased total size of the microglia suggests an increased proportion of ramified M1 type microglia responding to the injury.

3.3. IUO exposure alters metabolite signatures in the cortex

Metabolites in the brain are regulated in a spatiotemporal manner during critical neurodevelopmental periods to meet energy demands placed on the brain. We previously reported that rats which were exposed *in utero* to oxy showed distinct alterations in brain metabolites

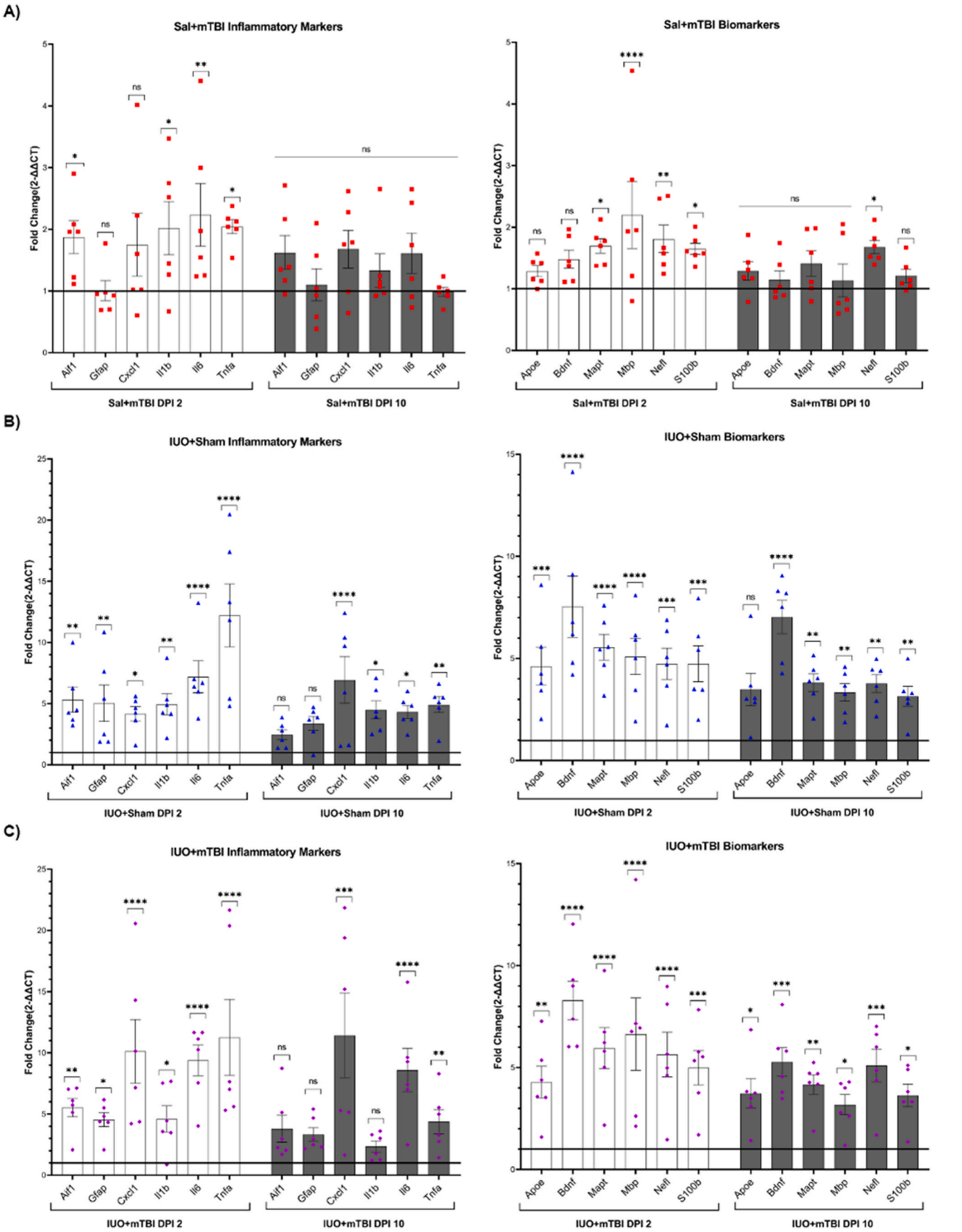

(caption on next page)

Fig. 2. Common gene markers of inflammation and brain injury are increased in mTBI and IUO exposure. Cortical brain tissue was assessed for mRNA levels of key biomarkers of inflammation and brain injury at 2- and 10- days post mTBI/Sham procedures using quantitative real-time PCR analysis. **(A)** Sal + mTBI conditions showed a significant increase of inflammatory markers *Aif1*, *Il1b*, *Il6*, and *Tnfα* as well as increased markers of brain injury *Bdnf*, *Mapt*, *Nefl*, and *S100β*. However, these effects were largely ameliorated at DPI 10. Nefl was the only significantly increased marker at DPI 10. **(B)** IUO + Sham conditions showed a significant increase in all biomarkers of inflammation and injury at DPI 2. At DPI 10 once again all markers were significantly increased. No significant gender differences were found within groups. **(C)** For the IUO + mTBI group all markers were significantly increased at DPI 2. While at day 10 *Cxcl1*, *Il6*, *Tnfα*, *Apoe*, *Bdnf*, *Mapt*, *Mbp*, *Nefl*, and *S100β* were increased. No significant gender differences were noted within groups. Additionally, when comparing IUO + Sham to IUO + mTBI no significant differences were found. Data are displayed as Mean ± SEM; for all conditions equal number of sexes were used n = 6; *p ≤ 0.05, **p ≤ 0.001, ***p ≤ 0.005, ****p ≤ 0.0001. Analysis was performed by two-way ANOVA with Fisher's LSD.

(Odegaard et al., 2021). However, it is unknown how IUO exposed subjects would respond to a neurological insult such as mTBI which places acute energy demand on the brain. Accordingly, P30 animals at DPI 2 were assessed for levels of cortical metabolites by ^{1}H-MRS. Metabolites assessed were N-Acetyl-Aspartate (NAA), Alanine, Choline, Creatine, GABA, Glucose, Glutamate, Glutamine, Glycine, Lactate, Myoinositol, and Taurine. Out of these, NAA, myoinositol, lactate, and glucose showed significant differences in the IUO + mTBI condition as compared to Sal + Sham (Fig. 4). Both NAA and Myoinositol are clinically relevant biomarkers of patient outcomes across multiple neurological injuries and diseases (Voevodskaya et al., 2019; Ng et al., 2014; Tumati et al., 2013; Kantarci et al., 2002). Interestingly, only NAA, which originates from the mitochondria of neurons, was significantly decreased in both IUO + Sham (mean = 66.91 ± 9.656 p ≤ 0.0032) and IUO + mTBI (mean = 67.48 ± 10.373 p ≤ 0.0036) as compared to both saline conditions (Fig. 4). On the other hand, myoinositol which is predominantly located in glial cells, showed increased expression in the IUO + mTBI animals when compared to the Sal + Sham condition. A concomitant decrease in glucose, the precursor of myoinositol, was seen along with an increase in lactate expression. Intriguingly, increase in lactate and corresponding decrease in glucose is a characteristic hallmark of brain injury (Patet et al., 2016). Hence, the data suggests a significant metabolic stress in the IUO + mTBI condition as compared to the Sal + mTBI condition (Fig. 4). Total metabolite signal was not significantly affected between all conditions (Supplementary Fig. 4) suggesting no technical errors during the acquisition of the data.

3.4. Cortical synaptosomes display unique protein signatures

Cortical metabolomic data suggests that IUO + mTBI significantly alters metabolite expression in the brain. It is well known that synaptic structures are the most active metabolic areas of the neuron. In order to further understand whether changes in brain metabolism affects synaptic function, we first evaluated the proteomic profile of cortical synaptosomes (SYP), pinched off nerve terminals that represent an important component in neurotransmission and synaptic plasticity (Evans, 2015; Whittaker et al., 1964; Bai and Witzmann, 2007). We purified cortical SYP from animals at DPI 2 and performed high-throughput quantitative mass spectrometry to characterize the synaptic proteome. A consistent number of total proteins were identified for all comparisons (Supplementary Table 3) suggesting controlled and unbiased analysis for all comparisons. By further employing a criterion of ≥2 unique peptides and a p ≤ 0.05 we were able to identify differentially expressed proteins (DiffExpPro) (Supplementary Table 4). DiffExpPro between Sal + mTBI, IUO + Sham, and IUO + mTBI as compared to Sal + Sham shows some overlapping, but mostly distinct DiffExpPro profiles for each condition (Fig. 5a, Supplementary Table 5). Only 5 proteins were found to be shared between the three conditions as compared to Sal + Sham: CYP51A1, HEXB, MGLL, TMEM256, and ZC2HC1A. Sal + mTBI conditions had 8 proteins which overlapped with IUO + mTBI conditions: SCRN1, ATXN10, SEC13, PIK3R4, PSMB4, SLC22A17, and DNM1L. No significant pathways were discovered in ClueGO or IPA analysis for these shared proteins (Supplementary Fig. 5a). However, between IUO + Sham and IUO + mTBI conditions, 88 proteins were shared (Fig. 5a). Since this is the largest number of overlapping proteins, we further performed functional analysis using ClueGO and heatmap. Results revealed that top hits (10 proteins), all of which were upregulated, were related to mitochondrial function (Fig. 5b). ClueGO analysis of the 88 shared proteins between the IUO conditions also revealed that they are involved in mitochondrial function and oxidative stress pathways (Fig. 5c). Interestingly, of the 88 shared proteins, 23 were directly related to mitochondrial function according to the MitoCarta3.0 database (Rath et al., 2021). Further, Ingenuity Pathway Analysis (IPA) identified a strong association between IUO exposure and mitochondrial dysfunction showing it as the most significantly associated pathway in IUO + Sham and the fifth most significant in IUO + mTBI conditions (Supplementary Figs. 5b and 5c). Further, we analyzed the shared upstream regulators for the IUO conditions. Results indicated that 5 of the top 10 regulators are known to be directly related to mitochondrial function or disease in the brain: HTT, RGS6, TFAM, NFU1, and KIT (Kang et al., 2018; Itoh et al., 2013; Bifsha et al., 2014; Invernizzi et al., 2014; Huang et al., 2014) (Supplementary Fig. 5d).

3.5. Identification of unique mitochondrial protein dysregulation in the cortical synapse

To further investigate mitochondrial proteins, we isolated both cortical tissue lysate (TL) and SYP protein from DPI 2, DPI 6 and DPI 10 animals and immunoblotted for all five primary mitochondrial complexes: NDUFB8 (CI), SDHB (CII), UQCRC2 (CIII), MTCO1 (CIV), and ATP5A (CV). These complex proteins were also indicated in our SYP proteomics data (Supplementary Fig. 6) Results indicated that at DPI 2 TL and SYP displayed unique profiles for each of the conditions (Figs. 6a & 7a). In TL Sal + mTBI was only significantly increased for CII protein SDHB as compared to Sal + Sham. Interestingly, TL from IUO + mTBI conditions displayed significantly increased levels of CIII and CV proteins as compared to both Sal + Sham, while in IUO + Sham conditions there was a significant increase in all five complexes (Fig. 6a). Further, at DPI 6, we see a significant return to Sal + Sham levels for both Sal + mTBI and IUO + Sham conditions (Fig. 6b). In IUO + mTBI conditions though a significant increase in CIII and CV protein levels was maintained through DPI 6. At DPI 10 in TL, we see non-significant differences for all complex in all conditions (Fig. 6c). On the other hand, SYP isolated from IUO + Sham conditions at DPI 2 displayed increased expression in mitochondrial complexes I-IV but not in complex V, while SYP isolated from IUO + mTBI conditions showed significantly increased levels for all five complexes when compared to Sal + Sham (Fig. 7a). Further, IUO + mTBI conditions also showed increased levels of CIII marker when compared to IUO + Sham (Fig. 7a). Similar to TL, in SYP at DPI 6 we see no significant differences between Sal + mTBI and IUO + Sham as compared to Sal + Sham conditions in any mitochondrial complex proteins (Fig. 7b). However, in IUO + mTBI conditions, we observed a significant upregulation of CII, CIII, and CV protein markers as compared to Sal + Sham. Interestingly, at DPI 10 in SYP, we see a significant decrease of complex protein levels in the IUO + mTBI conditions for CI, CII, CIV, and CV (Fig. 7c). In summary, we see a dynamic increase in mitochondria complex channel proteins in both IUO + Sham and IUO + mTBI conditions at DPI 2, but in the IUO + mTBI conditions these increases shifted to downregulation over the 10-day recovery window after mTBI. This data suggests that there is a dynamic and exacerbated response by synaptic mitochondria to mTBI in the IUO

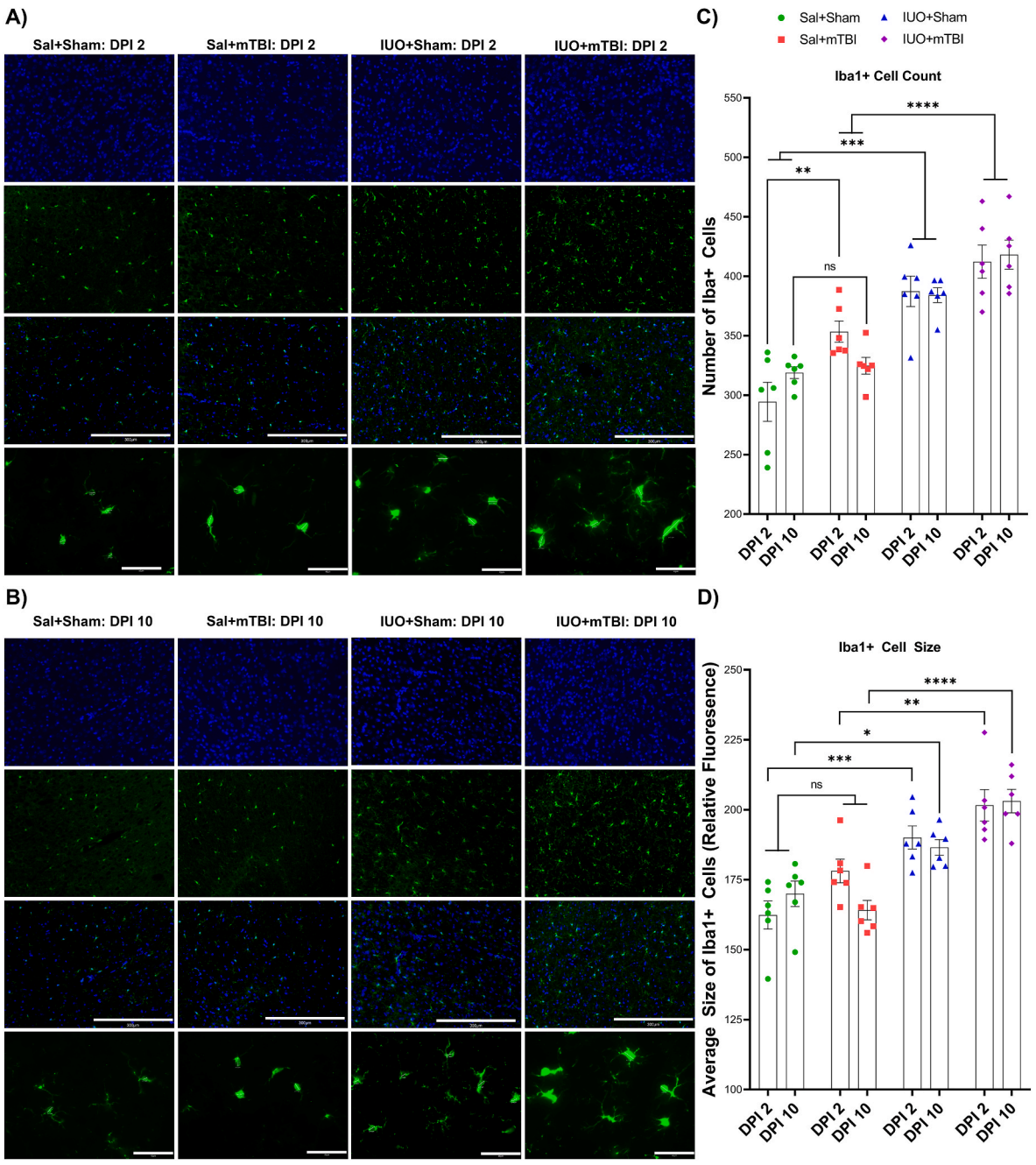

Fig. 3. Immunohistochemical analysis of cortical microglia/macrophages show that IUO exposure increases Iba1$^+$ number and cell size. Representative Iba1$^+$ stained sections at **(A)** DPI 2 and **(B)** DPI 10 from apical cortex for all four conditions shows increased number and size of Iba1+ cells in IUO conditions. **(C)** Quantification of total number of cells shows a significant increase in Sal + mTBI as compared to Sal + Sham at DPI 2 ($p \leq 0.0028$), but not at DPI 10 ($p > 0.98$). At DPI 2 and 10 both IUO + Sham and IUO + mTBI show increased number of Iba1+ cells when compared to Sal + Sham ($p \leq 0.001$), this significance is also observed in Sal + mTBI at DPI 10 for IUO + Sham ($p \leq 0.0026$) and IUO + mTBI ($p < 0.0001$). However, only IUO + mTBI was significantly increased at DPI 2 as compared to Sal + mTBI ($p \leq 0.0029$). **(D)** Quantification of the relative size of counted cells in Fig. 3c shows a trending but not significant increase in Iba1+ cell size in Sal + mTBI conditions as compared to Sal + Sham conditions at DPI 2 ($p > 0.0636$). IUO + Sham showed a significant increase in cell size when compared to Sal + Sham at DPI 2 ($p \leq 0.0003$) and DPI 10 ($p \leq 0.0461$), there was also a significant increase for IUO + mTBI at DPI 2 and DPI 10 ($p \leq 0.0001$). Further, IUO + mTBI showed a significant increase in Iba1+ cell size as compared to Sal + mTBI at DPI 2 ($p \leq 0.0023$) and DPI 10 ($p \leq 0.0001$). At DPI 10 IUO + mTBI Iba1+ cells were also significantly increased in size as compared to IUO + Sham conditions ($p \leq 0.0475$). For all conditions equal sexes were used ($n = 6$), and no significant gender differences were noted within groups. Data are displayed as Mean ± SEM (*$p \leq 0.05$; **$p \leq 0.001$; ***$p \leq 0.005$, ****$p \leq 0.0001$). Analysis was performed by two-way ANOVA with Tukey multiple comparison correction.

exposed subjects that rebounds during a 10-day recovery period. While equal number of genders were used, we did not find a significant difference in any gender comparisons except for MTCO1 at DPI 6 in the Sal + mTBI condition as compared to Sal + Sham (Supplementary Fig. 7).

3.6. Seahorse analysis of non-synaptic and synaptic mitochondrial respiration

To further investigate the role of mitochondria, we performed mitochondrial functional analysis using Seahorse Extracellular Flux

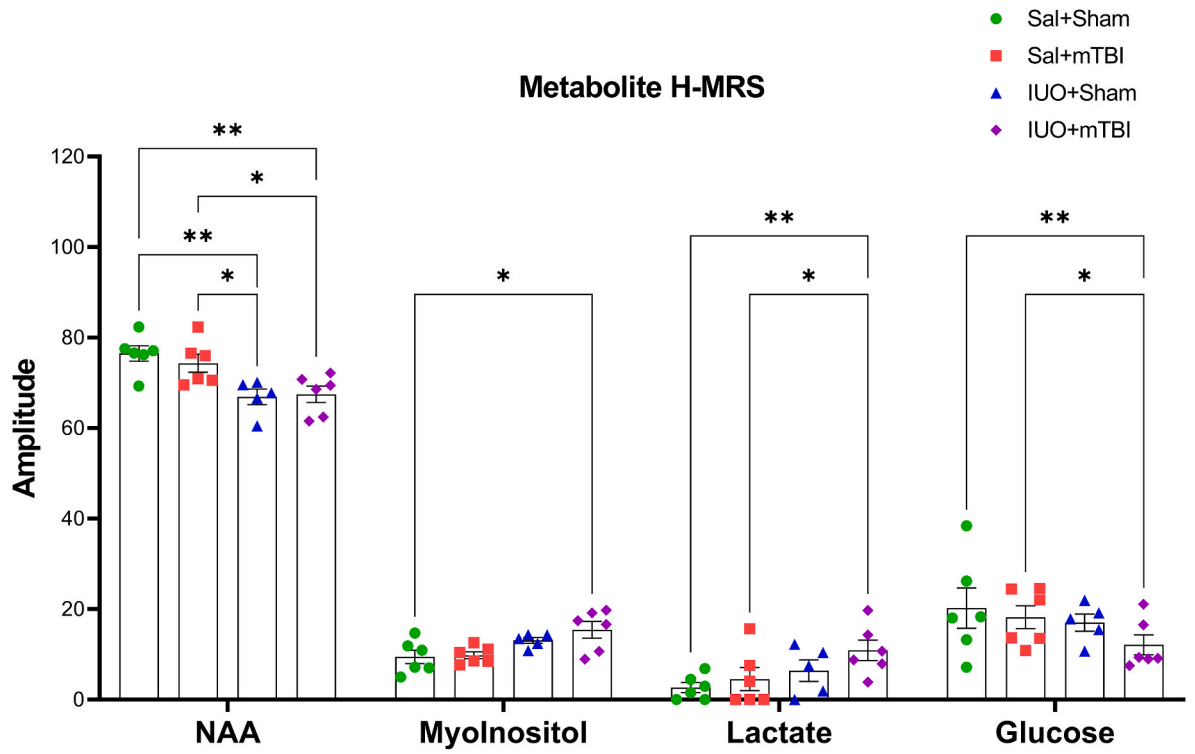

Fig. 4. ^{1}H-MRS to identify significantly altered metabolites in IUO + Sham and IUO + mTBI conditions. Metabolite signal is significantly affected in mitochondrially derived NAA for both IUO + Sham ($p \leq 0.003$) and IUO + mTBI conditions ($p \leq 0.0036$) as compared to Sal + Sham conditions. IUO + Sham ($p \leq 0.0217$) and IUO + mTBI ($p \leq 0.0259$) conditions also show decreased NAA as compared to Sal + mTBI conditions. Myoinositol ($p \leq 0.0499$), lactate ($p \leq 0.0076$), and glucose ($p \leq 0.0085$) are only significantly affected in IUO + mTBI conditions as compared to Sal + Sham. When comparing IUO + mTBI to Sal + mTBI only lactate ($p \leq 0.0383$) and glucose ($p \leq 0.0466$) are significantly altered. For Sal + Sham, Sal + mTBI, and IUO + mTBI, all numbers were balanced for sexes (n = 6, 3 males and 3 females) and for IUO + Sham, n = 3 males and n = 2 females were used. Data are displayed as Mean ± SEM; *$p \leq 0.05$; **$p \leq 0.001$; ***$p \leq 0.005$, ****$p \leq 0.0001$. Analysis performed by two-way ANOVA with Fisher's LSD.

Analyzer. First, mitochondria were isolated from SYP (SYPmito) and non-synaptic (NSYPmito) fractions from cortical brain tissue extracted from animals at DPI 2 and oxygen consumption rate (OCR) was measured in the presence of carbonyl cyanide-*p*-trifluoromethoxyphenylhydrazone (FCCP), an uncoupling agent known to disrupt ATP synthesis, while using pyruvate + malate to drive complex I function. Both SYPmito and NSYPmito isolated from Sal conditions showed no significant changes in both FCCP blocked basal respiration and pyruvate + malate driven maximal respiration (Fig. 8a and b). Results revealed that in response to mTBI, the NSYPmito from both the IUO + Sham and IUO + mTBI conditions had significantly increased basal and maximal OCR (Fig. 8a). However, the SYPmito in both IUO conditions found to have significantly increased maximal respiration but no difference at basal respiration (Fig. 8b). When calculating the individual complex OCR (subtracting background OCR of rotenone inhibited Complex I from basal respiration and Antimycin-A inhibited Complex III from succinate driven respiration), we identified complex specific effects. Both SYPmito and NSYPmito showed no differences in OCR among the Sal + mTBI conditions from Sal + Sham (Fig. 8a and b). In NSYPmito, only the IUO + Sham condition had significantly increased OCR in complex II and IV as compared to Sal + Sham, however, in the SYPmito, the IUO + mTBI conditions had significantly increased OCR in Complex II and IV but no differences in Complex I when compared to both Sal + Sham and Sal + mTBI conditions (Fig. 8a and b). While SYPmito isolated from IUO + Sham showed significantly increased Complex IV activity when compared to both Sal + Sham and Sal + mTBI conditions (Fig. 8b). To further investigate the long-term effects on mitochondrial function, we performed Seahorse analysis on animals that were recovering from DPI 38–40. At DPI 38–40 there were no significant differences discovered in NSYPmito OCR (Fig. 8c), however, in SYPmito OCR was significantly decreased when comparing IUO + Sham and IUO + mTBI conditions to Sal + Sham controls (Fig. 8d), showing an inverse effect as compared to DPI 2. Both Succinate and ASC/TMPD supported maximal respiration as well as basal respiration was significantly impaired in both IUO conditions as compared to Sal + Sham conditions suggesting an impairment of mitochondrial function in these animals (Fig. 8d). While investigating complex specific OCR, IUO + mTBI conditions showed significantly decreased SYPmito OCR in all three complexes (Fig. 8d). Further, a significant decrease was noted in the IUO + Sham conditions in Complex I (Fig. 8d). Together, these data suggest to us that in early development IUO exposure results in overactive synaptic mitochondrial respiration, additionally, over a longer period post injury, mitochondrial respiratory capacity is significantly impaired.

3.7. *Behavior analysis*

Our previous research found that IUO exposure showed minimal impact on social and anxiety-like behaviors in F1 generation but significant social impairments in the F2 generations (Odegaard et al., 2020a). Here, using the same methodology we sought to understand if IUO exposure and a later life injury such as mTBI would precipitate into behavioral deficits. To assess this, we performed marble burying, social novelty, and social preference experiments on all conditions between DPI 33–37 (Fig. 9a and b). We found that IUO conditions were significantly less likely to spend time in the compartment with a novel animal as opposed to a cagemate when compared to Sal + Sham animals (Fig. 9a). Interestingly though, despite the decreased time spent near the naïve animal in the IUO + mTBI conditions there was a significant increase in the number of entries into the naïve compartment but an unchanged number of touches by the IUO + mTBI condition (Fig. 9a). To

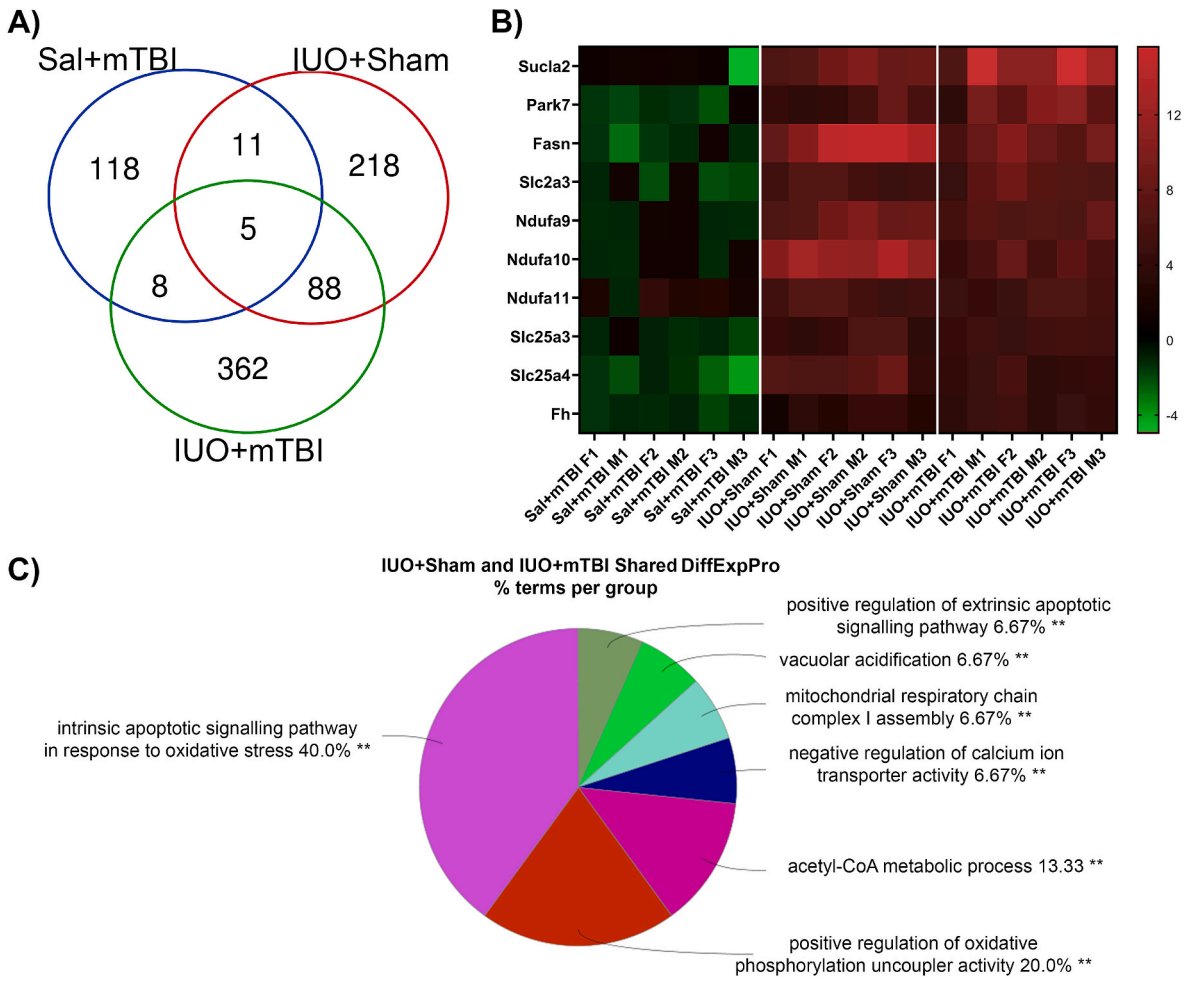

Fig. 5. Synaptic proteome identified by quantitative mass spectroscopy were associated with mitochondrial dysfunction in IUO conditions. (A) 88 overlapping DiffExpPro between IUO + Sham and IUO + mTBI conditions were found while only 8 were shared between Sal + mTBI and IUO + mTBI. Between all three groups, only five total DiffExpPro were shared as compared to Sal + Sham. **(B)** A heatmap of the top ten mitochondria associated DiffExpPro shows the significant overlap between IUO + Sham and IUO + mTBI in mitochondria proteins. **(C)** Clue-GO analysis of the 88 shared DiffExpPro between IUO + Sham and IUO + mTBI show a strong relationship to pathways associated with oxidative stress associated apoptosis, oxidative uncoupler activity, and respiratory complex I assembly. For all conditions, animals were balanced for sex (n = 6; 3 males and 3 females). (Clue-GO group term category *p ≤ 0.05; **p ≤ 0.001).

further understand this relationship, we assessed the number of touches per entry by all conditions and found that for IUO + mTBI conditions there were significantly lower number of touches per entry for the naïve animal, but not for the cagemate (Fig. 9a). We also performed social preference assessment comparing the desire to interact with a toy versus a novel animal (Fig. 9b). We found that in both IUO conditions the rats were again significantly less likely to spend time in the naïve animal's compartment and had decreased number of touches per entry (Fig. 9b). However, the IUO + Sham conditions were also significantly more likely to spend time near the toy and had greater number of touches despite having no difference in the number of attempted touches per entry with the toy; further, the IUO + Sham condition was also more likely to attempt to touch the toy (Fig. 9b). Beyond social deficits, NOWS children are also significantly more likely to suffer motor deficits and anxiety related behaviors (Odegaard et al., 2020a). Our social data suggests that IUO animals, despite having fewer interactions per entry, were highly active during the behavioral assessment which indicates anxiety-like motor patterns. To further understand this anxiety-like behavior we performed marble burying assessment for compulsive motor behavior and found that IUO + mTBI conditions were significantly more likely to perform marble burying than both Sal + Sham and Sal + mTBI conditions (Fig. 9c). To investigate the role of IUO and mTBI on motor function, we performed Rotarod assessment across six trials consisting of three learning trials and 3 test trials (Fig. 9d). We noted significant and consistent decrease in motor function in both IUO + Sham and IUO + mTBI conditions in trials 4, 5, and 6. Hot plate nociception tests were also performed at DPI 32 to investigate any nociceptive differences between groups prior to behavioral tests, however no significant differences were observed (Supplementary Fig. 8).

4. Discussion

It is well-known that prenatal drug exposure poses significant threat to the developing fetus, affecting overall brain development and consequently leading to maladaptive behaviors (Odegaard et al., 2020a, 2020b; Ross et al., 2015). Moreover, additional risk factors such as age of parents, education, and other stressors such as mild brain injury caused by slips and falls in infants can exacerbate these neurodevelopmental deficits. In this study, we utilized mTBI as a model to recapitulate these events in juvenile rats showing for the first time that prenatal oxycodone exposure can induce vulnerability to one of the most common childhood injuries. Specifically, that significant acute inflammation and metabolic dysregulation is accompanied by longitudinal metabolic dysfunction in the cortical synaptic microenvironment and behavioral perturbations. Together our results show that cumulative impact of a common child-hood injury, mTBI, can cause molecular and

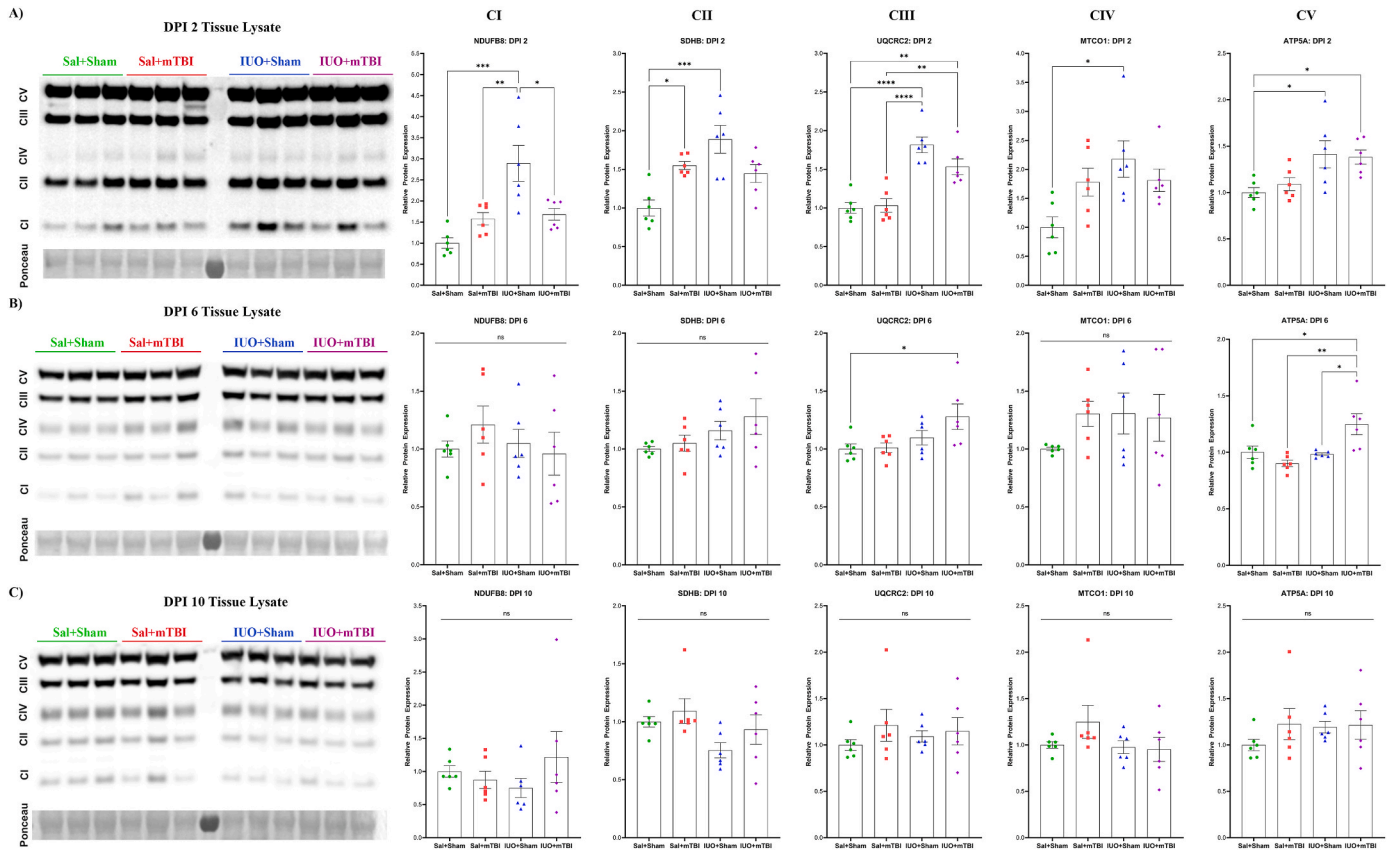

Fig. 6. Western blotting conducted on cortical tissue lysates found acute but not longitudinal alterations in the expression of oxidative phosphorylation complex proteins. (A) At DPI 2 significant increase in complex proteins were noted in TL for IUO + Sham conditions in all five complex proteins. Significant increase in complex proteins in TL for IUO + mTBI conditions in CI, CIII, and CV. **(B)** At DPI 6 in TL a significant increase in complex proteins was only noted in IUO + mTBI conditions for CIII and CV as compared to Sal + Sham. **(C)** At DPI 10 no changes in complex proteins could be seen in TL. Spectral protein values from cortical tissue lysates were normalized to ponceau staining and then data was compared to Sal + Sham conditions. For all conditions equal sexes were used (n = 6). Data are displayed as Mean ± SEM; *p ≤ 0.05; **p ≤ 0.001; ***p ≤ 0.005, ****p ≤ 0.0001. Analysis performed by one-way ANOVA with Tukey multiple comparison correction.

behavioral alterations to IUO exposed animals that would not otherwise be significant with IUO or mTBI insults alone.

Our first observations show that IUO exposed animals suffered decreased head diameter (Fig. 1), a condition often associated with cortical thinning and developmental deficits in NOWS children (Hartwell et al., 2020). Prescription opioid exposure has shown significant decrease in cortical volume of both left and right precentral gyrus, a region of the brain critical for motor function (Hartwell et al., 2020). This deficiency in the precentral gyrus has also been implicated in significant motor deficiencies in children diagnosed with NOWS, particularly, prevalent in children from the ages of 4.5–6 years old (Yeoh et al., 2019). An additional consideration is the behavior of the dams while on oxy as rearing behavior is known to impact brain and behavior (Labella et al., 2021; Wallin et al., 2021). While other studies in rats have found impairments in maternal care behaviors such as nursing and vocalization, we found no significant differences in pup-retrieval behavior between oxy dosed dams vs saline (Supplementary Fig. 9) (Schlagal et al., 2021). However human caretaking and nurturing patterns are much more intricate than multiparous murine models suggest that this is a confounding factor for many NOWS children (Velez et al., 2021). Next, we induced mTBI at P28 after 7 days without any oxycodone exposure through maternal breastmilk, which translates to a neurodevelopmental human age of a ~5-year-old (Semple et al., 2013; Tsujimoto, 2008). At 5 years old not only are NOWS children still suffering from motor deficits, but this is also one of the most vulnerable ages for juvenile mTBI due to slips, falls, and accidents during play (Yeoh et al., 2019; Taylor et al., 2017; Araki et al., 2017). To measure some of the subtle motor changes immediately post-mTBI, we quantitated righting reflex or time to right (the time each rat took to right itself from a supine to prone position after anesthesia) in the juvenile rats (Fig. 1c). Righting reflex has long been used as a measure of outcomes post-mTBI and directly suggests severity of injury in regards to both cellular and behavioral measures (Grin'kina et al., 2016). Our IUO + mTBI condition had revealed a significant impairment in TTR as compared to their Sal + mTBI counterparts, suggesting that IUO exposure rendered a significant vulnerability to brain injury (Fig. 1c). Increased TTR latency can be representative of multiple potential issues in the brain such as inflammatory response, synaptic depolarization, and mitochondrial dysfunction but all are suggestive that injury was more severe in IUO exposed animals (Grin'kina et al., 2016; Rowe et al., 2020; Creeley et al., 2004; Mashour et al., 2021).

Next, we sought to validate potential molecular mechanisms underlying this differential response to injury by investigating gene expression changes of common markers for inflammation and mTBI. Interestingly, our results showed a stark overlap of increased expression of genes associated with brain injury in IUO conditions. While our Sal + mTBI group did show an increased expression in some genes such as *Il1b*, *Il6*, *Tnfα, Mapt, Mbp, Nefl, and S100b,* these markers returned to baseline by DPI 10 apart from *Nefl*. This is not surprising as in healthy pediatric populations only 2.3% of patients experience longitudinal symptoms after an mTBI (Barlow et al., 2010). Further, in both human data and murine models of mTBI significant improvement of proinflammatory cytokines have been shown to recover significantly by DPI 6 (Helmy et al., 2011, 2012; Shojo et al., 2010). Intriguingly, the only marker of

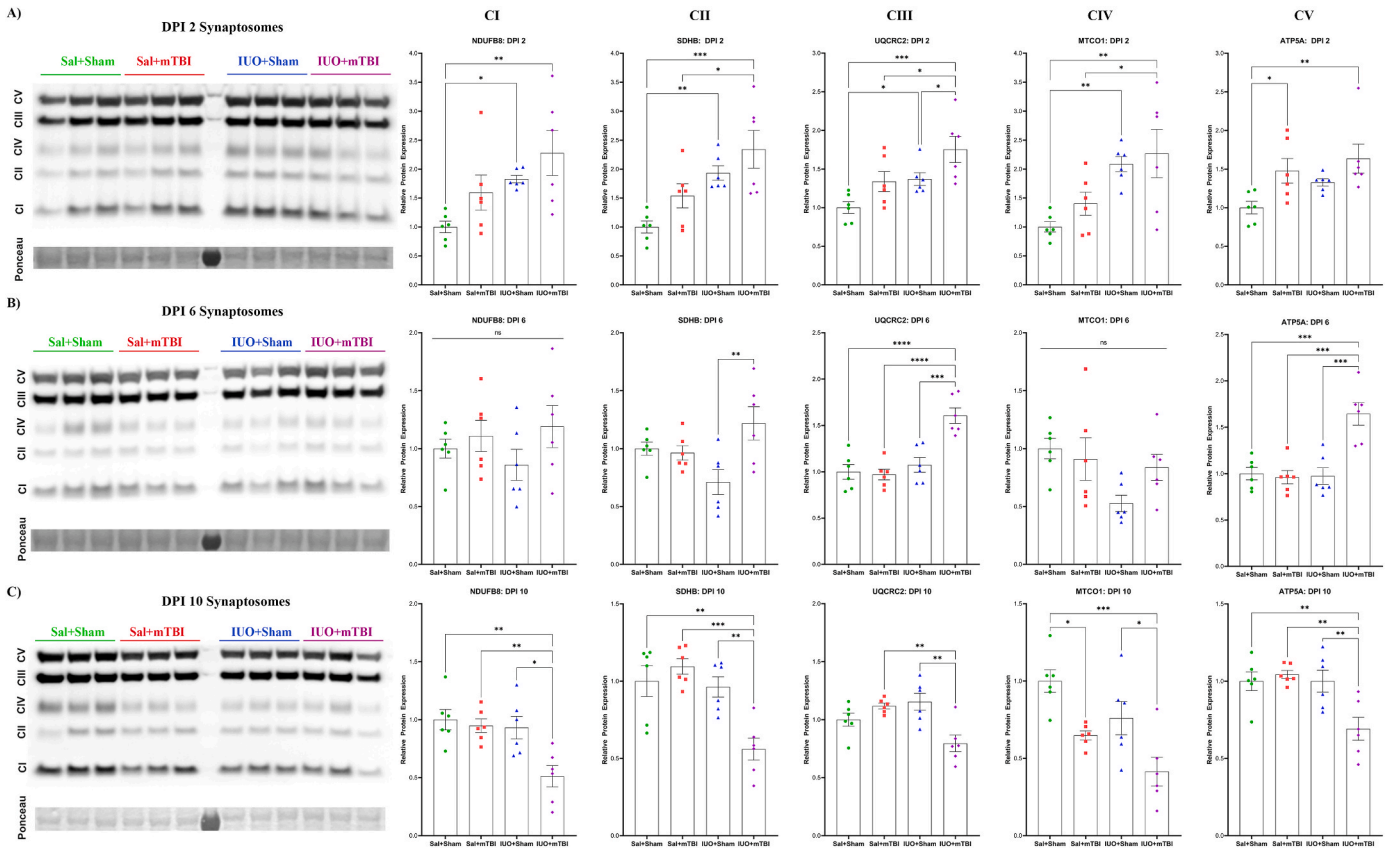

Fig. 7. Western blotting conducted on cortical synaptosomes found time specific alterations in the expression of oxidative phosphorylation complex proteins. (A) At DPI 2 significant increase in complex proteins were noted in SYP for IUO + Sham conditions in complexes I, II, III, and IV proteins as compared to Sal + Sham conditions. Significant increase in complex proteins in SYP for IUO + mTBI conditions in all five complex proteins as compared to Sal + Sham. Further, in complexes II, III, and IV IUO + mTBI conditions were also significantly increased as compared to Sal + mTBI. **(B)** At DPI 6 in SYP a significant increase in complex proteins was only noted in IUO + mTBI conditions for CIII and CV as compared to all other conditions. Interestingly, in complex II protein SDHB IUO + mTBI was significantly increased as compared to IUO + Sham only. **(C)** At DPI 10 a significant decrease in complex IV protein MTCO1 was noted in Sal + mTBI conditions as compared to Sal + Sham conditions. Further, lower levels could be seen in IUO + mTBI conditions as compared to all other conditions for Complexes I, II, and V. Additionally, IUO + mTBI conditions had lower levels of complex III and IV proteins as compared to IUO + Sham conditions. Spectral protein values from cortical synaptosomes were normalized to ponceau staining and then data was compared to Sal + Sham conditions. For all conditions equal sexes were used (n = 6). Data are displayed as Mean ± SEM; *p ≤ 0.05; **p ≤ 0.001; ***p ≤ 0.005, ****p ≤ 0.0001. Analysis performed by one-way ANOVA with Tukey multiple comparison correction.

mTBI significantly increased at DPI 10 in Sal + mTBI conditions was *Nefl,* which has been reported as a long-term indicator of axonal injury in mTBI patients (Graham et al., 2021). However, in both IUO + Sham and IUO + mTBI conditions increased levels almost all markers persisted through to DPI 10 (Fig. 2). This sustained increase only in the IUO conditions suggests that prenatal oxy exposure not only induces chronic inflammation but also, exacerbates inflammatory responses to subsequent mild brain injury. Previous works have shown that neuroinflammation is not only associated with opioid dependence but also with IUO exposure, and furthermore found that gestational opioid exposure induces functional brain injury (Zhang et al., 2017; Jantzie et al., 2020b). Further, an increase in expression of *Apoe* and *Mbp* in IUO conditions are in support of previous research works that also reported elevated levels during gestational opioid exposure (Sanchez et al., 2008; Pappas et al., 2015). Next, we also found an increased microglial recruitment as well size in the cortex of IUO exposed animals that remained consistent through DPI 10 when compared to Sal animals (Fig. 3). These Iba1+ cells could also be from invading macrophages, particularly since mTBI is known to disrupt the BBB and allow for increased peripheral macrophage activity leading to increased inflammation (Gadani et al., 2015). Our data clearly illustrates that a mild brain injury, which under normal circumstances is completely recoverable, could lead to a series of damaging molecular events in IUO exposed individuals. IUO exposure elicits an increased basal neuroinflammatory response, which has been previously reported, but also that this inflammation is increased in post-mTBI suggesting that, potentially, these IUO exposed subjects cannot respond appropriately to a brain injury. Additionally, the increased recruitment of microglia is associated with the onset of neurodegenerative pathogenesis seen in Alzheimer's Disease (Hansen et al., 2018). Interestingly we also see significantly increased *Mapt* expression in our qRT-PCR assay in IUO exposed conditions. Mapt is a protein whose pathological expression is directly involved in Alzheimer's Disease pathogenesis (Dubois et al., 2016). Together, this data suggests that IUO exposed brain is not only more vulnerable to injury but is also displaying early markers of neurodegenerative disease progression. It has long been established that brain injury leads to increased risk for neurodegenerative and dementia related diseases (Graham and Sharp, 2019). This comorbidity could explain the immune overlap in our IUO model with markers of both brain injury and Alzheimer's Disease. In summary, our data strongly suggests that IUO exposure creates a vulnerable environment in the brain, which, when challenged with another stressful event during development, such as mTBI, could potentially exacerbate neurological complications in later life. While these works focus on acute and longitudinal sequelae ranging between comparative murine ages of childhood and young adulthood, future studies should address NOWS models

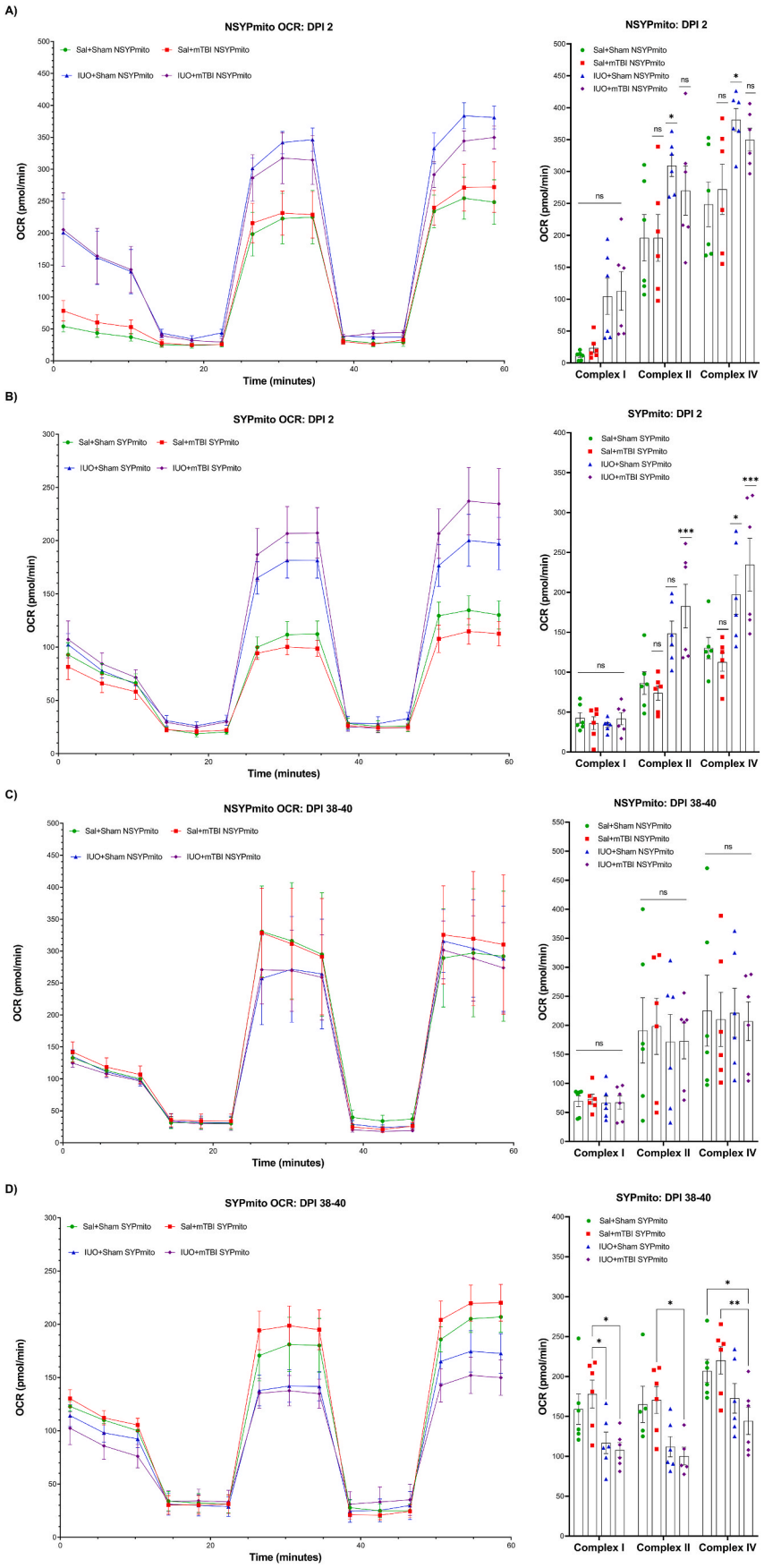

Fig. 8. Oxygen consumption rate of NSYPmito and SYPmito showed acutely increased respiration in SYPmito, but longitudinally decreased respiration by DPI 38–40. **(A)** At DPI 2, NSYPmito displayed significantly increase basal and maximal respiration in both IUO conditions. However, only IUO + Sham showed an increased Complex II and Complex IV respiration. **(B)** At DPI 2 SYPmito displayed significantly increase maximal respiration but no change in basal respiration. IUO + Sham showed increased Complex IV associated respiration while IUO + mTBI conditions showed increased Complex II and Complex IV associated respiration. **(C)** At DPI 38–40, no significant changes were seen in basal, maximal, or complex specific respiration among all conditions. **(D)** At DPI 38–40, a significant decrease in maximal respiration was seen in both IUO conditions, however, only IUO + mTBI displayed a significant decrease in basal respiration as compared to both saline groups. IUO + Sham and IUO + mTBI showed a significant decrease in Complex I respiration as compared to Sal + mTBI condition. IUO + mTBI further showed a decreased respiration as compared to Sal + mTBI for Complex II associated OCR. IUO + mTBI also showed a decreased respiration as compared to both saline conditions for Complex IV associated respiration. For all conditions equal sexes were used (n = 6) and one Sal + Sham animal was run in each plate. Data are displayed as Mean ± SEM; *p ≤ 0.05; **p ≤ 0.001; ***p ≤ 0.005, ****p ≤ 0.0001. Analysis performed by two-way ANOVA with Tukey multiple comparison correction.

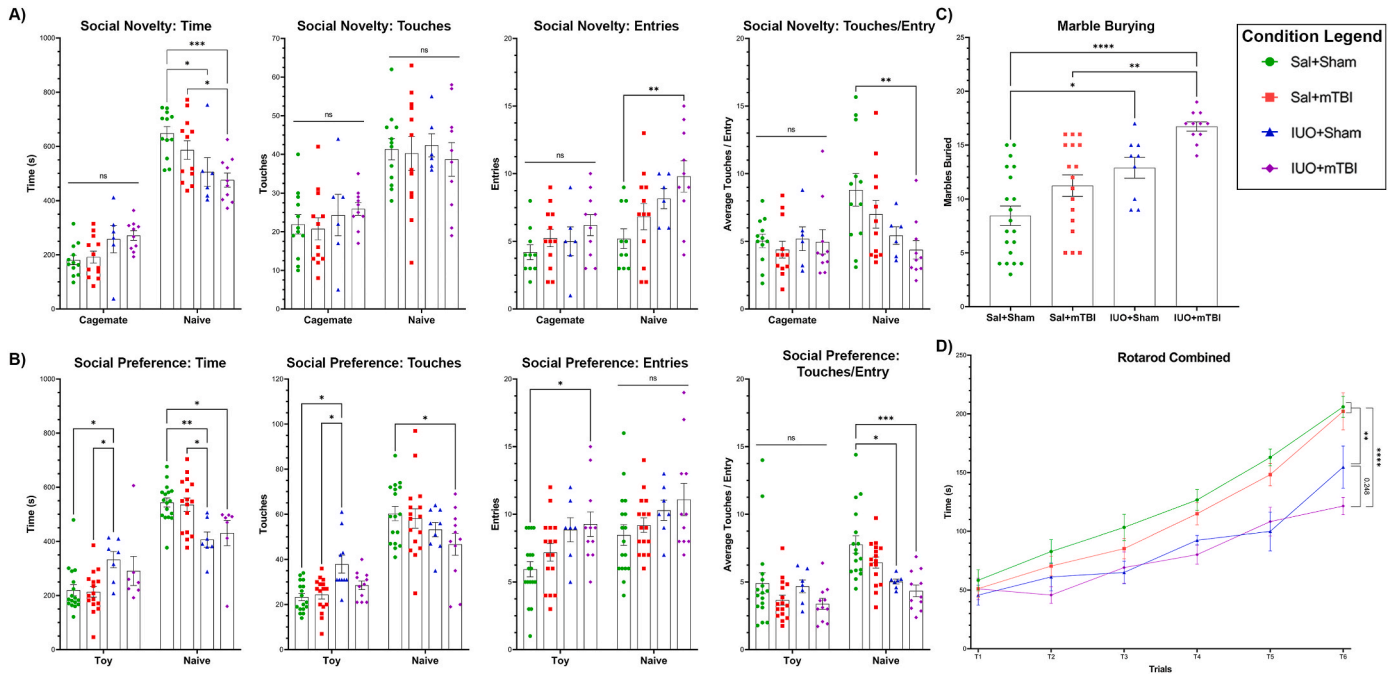

Fig. 9. Behavioral analysis found impairments in social, anxiety, and motor behaviors in IUO + mTBI conditions. (A) Social novelty testing showed no changes in sociality for Sal + mTBI conditions as compared to Sal + Sham. No changes were observed in cagemate interactions in all conditions. Naïve animal time spent was significantly decreased in both IUO conditions as compared to Sal + Sham. IUO + mTBI animals displayed significantly increased number of naïve animal compartment entries, but a significantly decreased number of touches per entry. **(B)** Social preference testing showed no changes in sociality for Sal + mTBI conditions as compared to Sal + Sham. IUO + Sham animals spent more time in the toy compartment and attempted more touches while also spending significantly less time in the Naïve animal compartment and attempting less naïve touches per entry. IUO + mTBI condition spent significantly less time in the Naïve animal compartment and attempting less naïve touches per entry. **(C)** Marble burying assessment of anxiety and compulsive like behavior showed the IUO + Sham animals buried more marbles than Sal + Sham conditions but a non-significantly different amount as compared to Sal + mTBI. IUO + mTBI buried significantly more marbles as compared to both Sal + Sham and Sal + mTBI. **(D)** Rotarod assessment showed a significant decrease in latency to fall in both IUO conditions in trials 5 and 6 as compared to both Sal + Sham and Sal + mTBI. No significant differences were observed in trials 1, 2, and 3. Data are displayed as Mean ± SEM; *p ≤ 0.05; **p ≤ 0.001; ***p ≤ 0.005, ****p ≤ 0.0001. Analysis performed by one-way ANOVA with Tukey multiple comparison correction for 9a, 9 b, and 9c. 9 d analysis performed by two-way mixed-model ANOVA with Tukey multiple comparison correction.

in the context of the aging brain as it is possible that NOWS children are not only vulnerable to mTBI, but also more vulnerable to developing mTBI induced onset of neurodegeneration and dementia.

Another key factor in the brain's response to an mTBI, both from an inflammatory and functional perspective, is metabolic dysfunction which is also known to affect loss of consciousness and impaired righting reflex (Giza and Hovda, 2001). Our findings show significant decrease in the mitochondrial derived metabolite NAA in IUO exposed animals (Fig. 4). Decreased NAA is directly associated with decreased levels of ATP and metabolic imbalance after brain injury, and seeing similar profiles in IUO exposure suggests that gestational oxy exposure disrupts mitochondrial and metabolic function in brain (Tavazzi et al., 2005; Signoretti et al., 2010; Metabolic Acetate Therapy for the, 2010). Further, increased myoinositol levels in IUO + mTBI conditions is intriguing as myoinositol is a clinical biomarker of outcomes post-mTBI in human patients (Fig. 4) (Voevodskaya et al., 2019). Myoinositol serves as a biomolecular intermediary in many neurotransmitters and hormones, a decrease would therefore suggest a dysfunction in neuronal signaling post-injury. Further, myoinositol is derived from glucose which also shows significant decrease alongside with a concomitant increase in lactate in only IUO + mTBI conditions. The dysregulation of both, predominantly, glial derived myoinositol and neuron derived NAA suggests that metabolic distress is not necessarily cell-type specific, but rather whole-brain. Interestingly, the level of glucose decrease has been previously reported to be relative to the degree of injury (Yoshino et al., 1991; Bergsneider et al., 1997). Even more alarming is that pediatric populations are particularly vulnerable to mTBI related glucose crisis as glucose metabolism peaks at approximately 5 years old to over 200% of adult glucose metabolism levels (Prins, 2017). Lactate has long been identified as an alternative to glucose, acting as a reserve fuel source in brain injury (Glenn et al., 2015). Increased lactate use by neurons has been shown to promote reactive oxygen species (ROS) production and subsequent oxidative stress (Jia et al., 2021; Yang and Lian, 2020; Corkey and Deeney, 2020). Metabolically induced oxidative stress in response to mTBI among IUO exposed subjects could be responsible for both the inflammatory response and impaired righting reflex. In summary, data so far strongly suggests that the IUO exposed brain is particularly incapable to meet energy demands post-injury and hence led us to investigate the most metabolically active unit of the brain, the synapse.

Quantitative proteomics of purified cortical synaptosomes revealed a strong relationship between IUO exposure and mitochondrial dysfunction. Bioinformatic analysis using ClueGO tool revealed a total of 88 shared DiffExpPro between IUO + Sham and IUO + mTBI identifying pathways for apoptotic signaling in response oxidative stress, regulation of oxidative stress, and acetyl-CoA metabolism (Fig. 5c). Intriguingly, acetyl-CoA is the immediate precursor to NAA and many pathophysiological abnormalities associated with lower NAA are thought to be caused by loss of acetyl-CoA (Vagnozzi et al., 2005). The observed relationship between molecular pathways associated with acetyl-CoA metabolism further validates the significance of the decreased NAA levels in both IUO exposure conditions. Further with IPA analysis, we found that metabolic and mitochondrial functional pathways are perturbed specifically in IUO + mTBI conditions. This includes signaling pathways associated with Huntington's Disease where regulators TFAM and HTT were found to be upregulated in IUO + mTBI conditions (Supplementary Figs. 5c and d). The nuclear-encoded regulatory protein TFAM which was strongly identified in our proteomics data is critical in

regulation of mtDNA replication, transcription, and packaging (Kang et al., 2018). In chronic neurological disease states, such as late-stage Huntington's Disease or Parkinson's Disease, TFAM levels are typically lower and thought to be caused by increased oxidative damage, however our proteomics data show TFAM levels are significantly elevated in the IUO + mTBI SYP. Increased TFAM levels have been shown to be neuroprotective in multiple studies investigating metabolic diseases of the brain in both human and rat models (Zhong et al., 2011; Hayashi et al., 2008; Morimoto et al., 2012; Oka et al., 2016). An increase (~2 fold) in TFAM could explain a possible compensatory mechanism for the increased energy demand in response to both IUO exposure and a brain injury. Chronic TFAM driven respiratory compensation in response to injury may become rapidly pathophysiologic during aging (Kang et al., 2018; Tuppen et al., 2010). Future studies investigating mtDNA regulation, specifically TFAM in aged subjects who were exposed to opioids prenatally, might shed light into new mechanisms and pathways to investigate dementia related diseases. IPA analysis also revealed increase in proteins relating to insulin secretion signaling pathways, mitochondrial dysfunction, and synaptic signaling pathways (Supplementary Fig. 5). Insulin resistance and other metabolic disorders have been heavily implicated in adult opioid misuse disorders, but have not been investigated sufficiently in neonatal exposure (Vagnozzi et al., 2005). However, insulin resistance is a known marker for mortality in cases of brain injury and is known to be exacerbated in response to brain injury (Sekar et al., 2021; Mowery et al., 2009). Interestingly, dysregulation of both synaptic signaling and insulin secretion pathways can be directly connected to mitochondrial dysfunction. Further, mitochondria play a significant role in inflammatory signaling and is a key regulator for many of the inflammatory genes noted in our qRT-PCR data: *Cxcl1*, *Il6*, *Il1β*, *Tnfα* (Fig. 2). In order to assess the role of the mitochondria in IUO exposure, we first analyzed the proteins in the mitochondrial oxidative phosphorylation complex (Figs. 6 and 7). We see that immediately after injury there is a dramatic increase in all mitochondrial complex proteins in both whole tissue lysate (TL) and synaptosomes (SYP), however, the levels came back to baseline in TL, but a significant decrease was observed in SYP (Figs. 6 and 7). Our data clearly suggests an increase in synaptic mitochondria function to keep up with the energy demands immediate post-injury and hence a decline in mitochondrial function was seen longitudinally (Fig. 8). The synaptosome represents a critical microenvironment of the brain which contains key neurotransmitters, pre- and post-synaptic membrane proteins, and a significant proportion of neural mitochondria (Whittaker, 1993). As such the synaptosome provides a window of insight into the key functional unit of the brain which has been implicated in several neurological vulnerabilities (Jamjoom et al., 2021). Traditional whole brain investigations might drown out the impacts given to this vulnerable microenvironment, and our data indicates that the synapse is specifically affected by IUO exposure. It is well known that the mitochondria at the synapse, both neural and astrocytic, are under extreme stress post-TBI (Jamjoom et al., 2020, 2021). Furthermore, IUO exposure exacerbates the effects of the injury as clearly demonstrated in the decreased levels of the mitochondrial proteins in the SYP (Figs. 6 and 7).

In order to further validate that IUO exposure causes significant mitochondrial stress, we assessed mitochondrial function. We observed no significant differences in oxygen consumption in either NSYPmito or SYPmito in the Sal + mTBI conditions suggesting that mitochondrial function is not significantly altered in mTBI alone (Fig. 8b and c). However, we did see a significant increase in complex II and IV oxygen consumption in NSYPmito at DPI 2 for IUO + Sham groups along with a trending increase in IUO + mTBI (Fig. 8a). This data dovetails with our previous observations in tissue lysate complex proteins at DPI 2, where we saw an increase in all complex proteins in IUO + Sham, however for IUO + mTBI we only identify significant changes in complexes III, IV, and V (Fig. 6a). Moreover, in IUO + mTBI conditions at DPI 2, SYPmito have significantly increased OCR in Complex II and IV while IUO + Sham conditions have a significantly increased OCR for only Complex IV (Fig. 8b). Again, this correlates with our Western blot data on complex proteins in SYP where, in all complexes, IUO + mTBI showed greater average levels of expression at DPI 2 (Fig. 7a). However, when assessing the mitochondria longitudinally we discovered that the increased OCR noted in juvenile subjects reversed by P66-67, specifically in synaptic mitochondria. IUO exposed subjects that suffered mTBI suffer more severe longitudinal consequences, resulting in impaired mitochondrial complexes I, II, and IV function (Fig. 8d). While there is a strong trend in IUO + Sham conditions towards impaired OCR in complexes I, II and IV as compared to Sal + Sham it does not reach significance. The history of investigating metabolic complexities and their relationship to mTBI should consider IUO exposure as an additional metabolic risk factor for worsened mTBI outocomes in this regard (Lai et al., 2022). Together, this data suggests that mitochondria hyperactivity caused by IUO exposure can become pathophysiological after mTBI. All together the data shows that both at molecular and functional level, IUO exposure causes mitochondrial stress and therefore dysfunction, specifically exacerbated in response to injury.

Furthermore, it has been extensively established that mitochondrial dysfunction and chronic inflammation are factors in known behavioral deficits associated NOWS such as autism, anxiety, social impairment, and motor deficiencies (Odegaard et al., 2020a; Ülgen et al., 2023; Rossignol and Frye, 2014; Misiewicz et al., 2019; Hollis et al., 2015; Picca et al., 2020). Interestingly, anxiety, social impairment, and motor dysfunction are also concomitant in pediatric brain injury (Perry et al., 2016; Zamani et al., 2019; Bigler et al., 2013; Ryan et al., 2021).

We sought to understand if mTBI would result in exacerbated NOWS associated behavioral changes in IUO exposed subjects at DPI 33–37. Many behavioral and functional deficits have been noted in children who had suffered from NOWS. Specifically, these children are significantly more likely to suffer social impediments including up to an 80% increased likelihood to develop autism by age 8 as well as a 68% increased chance to have developmental motor disorders (Weller et al., 2021). Our data showed that IUO exposed rats have impaired anxiety-like behavior, social preference behavior, and motor function (Fig. 9b, c, d). This data supports current epidemiological data in humans that show similar deficits in NOWS children (Weller et al., 2021). What is more fascinating is that a heightened effect is seen in the IUO + mTBI conditions. For example, in the IUO + mTBI conditions we see not only impaired preference to spend time with a naïve rat, but also an increased number of entries towards the naïve rats resulting in significantly impaired touches per entry for a naïve rat (Fig. 9a). This is again shown in the social preference experiment for both IUO + Sham and IUO + mTBI conditions (Fig. 9b). This suggests that animals exposed to both stressors, although exhibiting a curiosity to explore, failed to participate in social interaction indicating autistic-like behavioral patterns, where social interaction isn't unwanted just atypical (Umagami et al., 2022). Our marble burying data, which represents more generalized anxiety, also suggests that IUO exposure induces anxiety like behaviors which become exacerbated in IUO + mTBI conditions (Fig. 9c). Notably, no significant differences are seen in any behavioral measure in our Sal + mTBI conditions. Yet again our data supports that the damage caused by an mTBI, while normally fully recoverable, in IUO exposed subjects results in behavioral deficits. Specifically, these behavioral measures related to NOWS associated behavioral deficits are exacerbated in IUO exposed rats who suffer a juvenile mTBI. Furthermore, significantly impaired motor function seen in IUO conditions suggests that NOWS children are not only likely to be vulnerable to the sequelae of mTBI at the molecular level but may also be more likely to suffer an mTBI as young adults (Fig. 9d). This further supports human data which has found deficits in the size of the motor cortex of NOWS children and epidemiological data of greater ER admittance for injuries (Yeoh et al., 2019; Liu et al., 2019). Epidemiological data shows that NOWS children are significantly more likely to be admitted to the ED for injury than non-opioid exposed children (Cunha-Oliveira et al., 2008).

Considering that mTBI caused by slips, falls, and accidents during play, is one of the most common admittance reasons for children, the impaired motor control caused by IUO, could be considered as a contributing factor. In summary, our data shows that *in utero* opioid exposure not only renders the brain vulnerable to pediatric brain injury but also at the molecular level, causes significant neuroinflammation, alterations in brain metabolites, and synaptic mitochondria dysfunction that further precipitates into behavioral deficits observed in NOWS children.

5. Conclusion

In conclusion, our study provides, for the first time, robust and novel evidence that *in utero* oxycodone exposure results in long lasting molecular and behavioral deficits. These effects strongly represent deficiencies observed in children who suffered from neonatal opioid withdrawal syndrome as infants and our study identified specific molecular mechanisms behind these pathophysiologies. *In utero* oxycodone exposure results in increased neuroinflammation, aberrant metabolites, mitochondrial dysfunction, and impaired behavior. Each of these deleterious pathophysiological responses is further exacerbated by a normally recoverable minor traumatic brain injury. These results suggest that the growing population of individuals exposed prenatally to opioids is at tremendous risk to one of the most common pediatric injuries: mTBI. The role of the mitochondria in affecting this vulnerability appears to be at the forefront of not only the etiology, but also a strong potential therapeutic target for NOWS children.

Funding

This work is supported by the National Institutes of Health R01DA042379 (SVY)], DA049577 (G.P.), Lieberman Endowment (G.P) and Developmental funding provided by Department of Anesthesiology, University of Nebraska Medical Center (G.P. and S.V.Y). We also thank the Cognitive Neuroscience of Developmental and Aging (CoNDA) Center for the core facility voucher funding of H-MRS metabolite analysis to AG. The funding entity played no role in the study design or its conduction.

Declaration of competing interest

The authors declare that they have no known competing financial interests or personal relationships that could have appeared to influence the work reported in this paper.

Data availability

Data will be made available on request.

Appendix A. Supplementary data

Supplementary data to this article can be found online at https://doi.org/10.1016/j.bbih.2023.100669.

References

Andersen, S.L., 2003. Trajectories of brain development: point of vulnerability or window of opportunity? Neurosci. Biobehav. Rev. 27 (1–2), 3–18.
Araki, T., Yokota, H., Morita, A., 2017. Pediatric traumatic brain injury: characteristic features, diagnosis, and management. Neurol. Med.-Chir. 57 (2), 82–93.
Arciniegas, D.B., Wortzel, H.S., 2014. Emotional and behavioral dyscontrol after traumatic brain injury. Psychiatr. Clin. 37 (1), 31–53.
Asken, B.M., et al., 2016. Factors influencing clinical correlates of chronic traumatic encephalopathy (CTE): a review. Neuropsychol. Rev. 26 (4), 340–363.
Bai, F., Witzmann, F.A., 2007. *Synaptosome Proteomics.* Subcellular Proteomics: from Cell Deconstruction to System Reconstruction, pp. 77–98.
Bailey, B.A., et al., 2022. Impact of in utero opioid exposure on newborn outcomes: beyond neonatal opioid withdrawal syndrome. J. Matern. Fetal Neonatal Med. 35 (25), 9383–9390.
Barlow, K.M., et al., 2010. Epidemiology of postconcussion syndrome in pediatric mild traumatic brain injury. Pediatrics 126 (2), e374–e381.
Bergsneider, M., et al., 1997. Cerebral hyperglycolysis following severe traumatic brain injury in humans: a positron emission tomography study. J. Neurosurg. 86 (2), 241–251.
Bifsha, P., et al., 2014. Rgs6 is required for adult maintenance of dopaminergic neurons in the ventral substantia nigra. PLoS Genet. 10 (12), e1004863.
Bigler, E.D., et al., 2013. Neuroimaging and social behavior in children after traumatic brain injury: findings from the Social Outcomes of Brain Injury in Kids (SOBIK) study. NeuroRehabilitation 32 (4), 707–720.
Boggess, T., Risher, W.C., 2022. Clinical and basic research investigations into the long-term effects of prenatal opioid exposure on brain development. J. Neurosci. Res. 100 (1), 396–409.
Calvillo, M., Irimia, A., 2020. Neuroimaging and psychometric assessment of mild cognitive impairment after traumatic brain injury. Front. Psychol. 11, 1423.
Caplain, S., et al., 2017. Early detection of poor outcome after mild traumatic brain injury: predictive factors using a multidimensional approach a pilot study. Front. Neurol. 8, 666.
Carroll, L., et al., 2004. Prognosis for mild traumatic brain injury: results of the WHO collaborating centre task force on mild traumatic brain injury. J. Rehabil. Med. 36 (0), 84–105.
Cherry, J.D., et al., 2018. Variation in TMEM106B in chronic traumatic encephalopathy. Acta Neuropathologica Communications 6 (1), 115.
Concussions and Brain Injuries in Children: United States, 2020, 2021. S. National Center for Health, Hyattsville, MD. https://doi.org/10.15620/cdc:111174.
Corkey, B.E., Deeney, J.T., 2020. The redox communication network as a regulator of metabolism. Front. Physiol. 11, 567796.
Creeley, C.E., et al., 2004. Multiple episodes of mild traumatic brain injury result in impaired cognitive performance in mice. Acad. Emerg. Med. 11 (8), 809–819.
Cunha-Oliveira, T., Rego, A.C., Oliveira, C.R., 2008. Cellular and molecular mechanisms involved in the neurotoxicity of opioid and psychostimulant drugs. Brain Res. Rev. 58 (1), 192–208.
Dubois, B., et al., 2016. Preclinical Alzheimer's disease: definition, natural history, and diagnostic criteria. Alzheimers Dement 12 (3), 292–323.
Evans, G.J., 2015. The synaptosome as a model system for studying synaptic physiology. Cold Spring Harb. Protoc. 2015 (5), top074450.
Gadani, S.P., et al., 2015. Dealing with danger in the CNS: the response of the immune system to injury. Neuron 87 (1), 47–62.
Giza, C.C., Hovda, D.A., 2001. The neurometabolic cascade of concussion. J. Athl. Train. 36 (3), 228–235.
Glenn, T.C., et al., 2015. Lactate: brain fuel in human traumatic brain injury: a comparison with normal healthy control subjects. J. Neurotrauma 32 (11), 820–832.
Graham, N.S., Sharp, D.J., 2019. Understanding neurodegeneration after traumatic brain injury: from mechanisms to clinical trials in dementia. J. Neurol. Neurosurg. Psychiatr. 90 (11), 1221–1233.
Graham, N.S.N., et al., 2021. Axonal marker neurofilament light predicts long-term outcomes and progressive neurodegeneration after traumatic brain injury. Sci. Transl. Med. 13 (613), eabg9922.
Grin'kina, N.M., et al., 2016. Righting reflex predicts long-term histological and behavioral outcomes in a closed head model of traumatic brain injury. PLoS One 11 (9), e0161053.
Hall, E.S., Meinzen-Derr, J., Wexelblatt, S.L., 2015. Cohort analysis of a pharmacokinetic-modeled methadone weaning optimization for neonatal abstinence syndrome. J. Pediatr. 167 (6), 1221, 5.e1.
Hansen, D.V., Hanson, J.E., Sheng, M., 2018. Microglia in Alzheimer's disease. J. Cell Biol. 217 (2), 459–472.
Hartwell, M.L., et al., 2020. Association of prenatal opioid exposure with precentral gyrus volume in children. JAMA Pediatr. 174 (9), 893–896.
Hayashi, Y., et al., 2008. Reverse of age-dependent memory impairment and mitochondrial DNA damage in microglia by an overexpression of human mitochondrial transcription factor a in mice. J. Neurosci. 28 (34), 8624–8634.
Helmy, A., et al., 2011. The cytokine response to human traumatic brain injury: temporal profiles and evidence for cerebral parenchymal production. J. Cerebr. Blood Flow Metabol. 31 (2), 658–670.
Helmy, A., et al., 2012. Principal component analysis of the cytokine and chemokine response to human traumatic brain injury. PLoS One 7 (6), e39677.
Hollis, F., et al., 2015. Mitochondrial function in the brain links anxiety with social subordination. Proc. Natl. Acad. Sci. USA 112 (50), 15486–15491.
Huang, Z., et al., 2014. The stem cell factor/Kit signalling pathway regulates mitochondrial function and energy expenditure. Nat. Commun. 5 (1), 4282.
Invernizzi, F., et al., 2014. Cavitating leukoencephalopathy with multiple mitochondrial dysfunction syndrome and NFU1 mutations. Front. Genet. 5, 412.
Itoh, K., et al., 2013. Mitochondrial dynamics in neurodegeneration. Trends Cell Biol. 23 (2), 64–71.
Jamjoom, A.A.B., et al., 2020. The synapse in traumatic brain injury. Brain 144 (1), 18–31.
Jamjoom, A.A.B., et al., 2021. The synapse in traumatic brain injury. Brain 144 (1), 18–31.
Jantzie, L.L., et al., 2020a. Prenatal opioid exposure: the next neonatal neuroinflammatory disease. Brain Behav. Immun. 84, 45–58.
Jantzie, L.L., et al., 2020b. Prenatal opioid exposure: the next neonatal neuroinflammatory disease. Brain Behav. Immun. 84, 45–58.
Jia, L., et al., 2021. Rheb-regulated mitochondrial pyruvate metabolism of Schwann cells linked to axon stability. Dev. Cell 56 (21), 2980–2994 e6.
Johnson, V.E., et al., 2013. Inflammation and white matter degeneration persist for years after a single traumatic brain injury. Brain 136 (Pt 1), 28–42.

Kang, I., Chu, C.T., Kaufman, B.A., 2018. The mitochondrial transcription factor TFAM in neurodegeneration: emerging evidence and mechanisms. FEBS Lett. 592 (5), 793–811.
Kantarci, K., et al., 2002. 1H magnetic resonance spectroscopy, cognitive function, and apolipoprotein E genotype in normal aging, mild cognitive impairment and Alzheimer's disease. J. Int. Neuropsychol. Soc. 8 (7), 934–942.
Kuehn, B., 2018. Opioid use disorder during pregnancy. JAMA 320 (12), 1232, 1232.
Labella, M.H., et al., 2021. Adapting an evidence-based home visiting intervention for mothers with opioid dependence: modified attachment and biobehavioral catch-up. Front. Psychol. 12, 675866.
Lai, J.-q., et al., 2022. Metabolic disorders on cognitive dysfunction after traumatic brain injury. Trends Endocrinol. Metabol. 33 (7), 451–462.
Larson, J.J., et al., 2019. Cognitive and behavioral impact on children exposed to opioids during pregnancy. Pediatrics 144 (2).
Li, W., et al., 2016. Traumatic brain injury and age at onset of cognitive impairment in older adults. J. Neurol. 263 (7), 1280–1285.
Little, B., et al., 2021. Teratogenic effects of maternal drug abuse on developing brain and underlying neurotransmitter mechanisms. Neurotoxicology 86, 172–179.
Liu, G., et al., 2019. A longitudinal healthcare use profile of children with a history of neonatal abstinence syndrome. J. Pediatr. 204, 111–117 e1.
Mashour, G.A., et al., 2021. Recovery of consciousness and cognition after general anesthesia in humans. Elife 10, e59525.
McDonald, S.J., Shultz, S.R., Agoston, D.V., 2021. The known unknowns: an overview of the state of blood-based protein biomarkers of mild traumatic brain injury. J. Neurotrauma 38 (19), 2652–2666.
Merhar, S.L., et al., 2021. Prenatal opioid exposure is associated with smaller brain volumes in multiple regions. Pediatr. Res. 90 (2), 397–402.
Metabolic acetate Therapy for the treatment of traumatic brain injury. J. Neurotrauma 27 (1), 2010, 293–298.
Misiewicz, Z., et al., 2019. Multi-omics analysis identifies mitochondrial pathways associated with anxiety-related behavior. PLoS Genet. 15 (9), e1008358.
Morimoto, N., et al., 2012. Effect of mitochondrial transcription factor a overexpression on motor neurons in amyotrophic lateral sclerosis model mice. J. Neurosci. Res. 90 (6), 1200–1208.
Mowery, N.T., et al., 2009. Stress insulin resistance is a marker for mortality in traumatic brain injury. J. Trauma Acute Care Surg. 66 (1), 145–153.
Mychasiuk, R., et al., 2014. A novel model of mild traumatic brain injury for juvenile rats. J. Vis. Exp. (94).
Newville, J., et al., 2020. Perinatal opioid exposure primes the peripheral immune system toward hyperreactivity. Frontiers in Pediatrics 8, 272.
Ng, T.S., et al., 2014. Neuroimaging in repetitive brain trauma. Alzheimer's Res. Ther. 6 (1), 10.
Nguyen, N.M., et al., 2022. Decoding the synaptic proteome with long-term exposure to midazolam during early development. Int. J. Mol. Sci. 23 (8).
Odegaard, K.E., et al., 2020a. Characterization of the intergenerational impact of in utero and postnatal oxycodone exposure. Transl. Psychiatry 10 (1), 1–11.
Odegaard, K.E., et al., 2020b. A holistic systems approach to characterize the impact of pre- and post-natal oxycodone exposure on neurodevelopment and behavior. Front. Cell Dev. Biol. 8, 619199.
Odegaard, K.E., et al., 2020c. Characterization of the intergenerational impact of in utero and postnatal oxycodone exposure. Transl. Psychiatry 10 (1), 329, 329.
Odegaard, K.E., et al., 2021. A holistic systems approach to characterize the impact of pre-and post-natal oxycodone exposure on neurodevelopment and behavior. Front. Cell Dev. Biol. 8, 619199.
Oei, J.L., et al., 2017. Neonatal abstinence syndrome and high school performance. Pediatrics 139 (2).
Oka, S., et al., 2016. Human mitochondrial transcriptional factor A breaks the mitochondria-mediated vicious cycle in Alzheimer's disease. Sci. Rep. 6 (1), 37889.
Pappas, A., et al., 2015. Transcriptomics of maternal and fetal membranes can discriminate between gestational-age matched preterm neonates with and without cognitive impairment diagnosed at 18–24 months. PLoS One 10 (3), e0118573.
Patet, C., et al., 2016. Cerebral lactate metabolism after traumatic brain injury. Curr. Neurol. Neurosci. Rep. 16 (4), 31.
Perry, D.C., et al., 2016. Association of traumatic brain injury with subsequent neurological and psychiatric disease: a meta-analysis. J. Neurosurg. 124 (2), 511–526.
Picca, A., et al., 2020. Mitochondrial dysfunction, oxidative stress, and neuroinflammation: intertwined roads to neurodegeneration. Antioxidants 9 (8), 647.
Prins, M.L., 2017. Glucose metabolism in pediatric traumatic brain injury. Child's Nerv. Syst. 33 (10), 1711–1718.
Rath, S., et al., 2021. MitoCarta3.0: an updated mitochondrial proteome now with sub-organelle localization and pathway annotations. Nucleic Acids Res. 49 (D1), D1541–d1547.
Rickards, T.A., Cranston, C.C., McWhorter, J., 2022. Persistent post-concussive symptoms: a model of predisposing, precipitating, and perpetuating factors. Appl. Neuropsychol.: Adultspan 29 (2), 284–294.
Rogers, G.W., et al., 2011. High throughput microplate respiratory measurements using minimal quantities of isolated mitochondria. PLoS One 6 (7), e21746.
Ross, E.J., et al., 2015. Developmental consequences of fetal exposure to drugs: what we know and what we still must learn. Neuropsychopharmacology 40 (1), 61–87.
Rossignol, D.A., Frye, R.E., 2014. Evidence linking oxidative stress, mitochondrial dysfunction, and inflammation in the brain of individuals with autism. Front. Physiol. 5, 150.
Rowe, R.K., Ortiz, J.B., Thomas, T.C., 2020. Mild and moderate traumatic brain injury and repeated stress affect corticosterone in the rat. Neurotrauma Rep 1 (1), 113–124.
Ryan, N.P., et al., 2021. Executive function mediates the prospective association between neurostructural differences within the central executive network and anti-social behavior after childhood traumatic brain injury. JCPP (J. Child Psychol. Psychiatry) 62 (9), 1150–1161.
Sanchez, E.S., et al., 2008. Opioid addiction and pregnancy: perinatal exposure to buprenorphine affects myelination in the developing brain. Glia 56 (9), 1017–1027.
Schindelin, J., et al., 2012. Fiji: an open-source platform for biological-image analysis. Nat. Methods 9 (7), 676–682.
Schlagal, C.R., et al., 2021. Maternal opioid exposure culminates in perturbed murine neurodevelopment and hyperactive phenotype in adolescence. Neuroscience 463, 272–287.
Sekar, S., et al., 2021. Concussion/mild traumatic brain injury (TBI) induces brain insulin resistance: a positron emission tomography (PET) scanning study. Int. J. Mol. Sci. 22 (16), 9005.
Semple, B.D., et al., 2013. Brain development in rodents and humans: identifying benchmarks of maturation and vulnerability to injury across species. Prog. Neurobiol. 106–107, 1–16.
Shahjin, F., et al., 2019. Brain-derived extracellular vesicle microRNA signatures associated with in utero and postnatal oxycodone exposure. Cells 9 (1), 21.
Shannon, P., et al., 2003. Cytoscape: a software environment for integrated models of biomolecular interaction networks. Genome Res. 13 (11), 2498–2504.
Shojo, H., et al., 2010. Genetic and histologic evidence implicates role of inflammation in traumatic brain injury-induced apoptosis in the rat cerebral cortex following moderate fluid percussion injury. Neuroscience 171 (4), 1273–1282.
Shultz, S.R., et al., 2017. The potential for animal models to provide insight into mild traumatic brain injury: translational challenges and strategies. Neurosci. Biobehav. Rev. 76, 396–414.
Signoretti, S., et al., 2010. Biochemical and neurochemical sequelae following mild traumatic brain injury: summary of experimental data and clinical implications. Neurosurgical Focus FOC 29 (5), E1.
Tavazzi, B., et al., 2005. Cerebral oxidative stress and depression of energy metabolism correlate with severity of diffuse brain injury in rats. Neurosurgery 56 (3).
Taylor, C.A., et al., 2017. Traumatic brain injury–related emergency department visits, hospitalizations, and deaths—United States, 2007 and 2013. MMWR Surveillance Summaries 66 (9), 1.
Tsujimoto, S., 2008. The prefrontal cortex: functional neural development during early childhood. Neuroscientist 14 (4), 345–358.
Tumati, S., Martens, S., Aleman, A., 2013. Magnetic resonance spectroscopy in mild cognitive impairment: systematic review and meta-analysis. Neurosci. Biobehav. Rev. 37 (10), 2571–2586.
Tuppen, H.A., et al., 2010. Mitochondrial DNA mutations and human disease. Biochim. Biophys. Acta Bioenerg. 1797 (2), 113–128.
Tweedie, D., et al., 2020. Time-dependent cytokine and chemokine changes in mouse cerebral cortex following a mild traumatic brain injury. Elife 9.
Ülgen, D.H., Ruigrok, S.R., Sandi, C., 2023. Powering the social brain: mitochondria in social behaviour. Curr. Opin. Neurobiol. 79, 102675.
Umagami, K., et al., 2022. Loneliness in autistic adults: a systematic review. Autism 26 (8), 2117–2135.
Vagnozzi, R., et al., 2005. Hypothesis of the postconcussive vulnerable brain: experimental evidence of its metabolic occurrence. Neurosurgery 57 (1).
Vasan, V., et al., 2021. Neonatal opioid exposure: public health crisis and novel neuroinflammatory disease. Neural Regen Res 16 (3), 430–432.
Velez, M.L., Jordan, C., Jansson, L.M., 2021. Reconceptualizing non-pharmacologic approaches to Neonatal Abstinence Syndrome (NAS) and Neonatal Opioid Withdrawal Syndrome (NOWS): a theoretical and evidence–based approach. Part II: the clinical application of nonpharmacologic care for NAS/NOWS. Neurotoxicol. Teratol. 88, 107032.
Voevodskaya, O., et al., 2019. Brain myoinositol as a potential marker of amyloid-related pathology: a longitudinal study. Neurology 92 (5), e395–e405.
Wallin, C.M., Bowen, S.E., Brummelte, S., 2021. Opioid use during pregnancy can impair maternal behavior and the Maternal Brain Network: a literature review. Neurotoxicol. Teratol. 86, 106976.
Weller, A.E., et al., 2021. Neonatal opioid withdrawal syndrome (NOWS): a transgenerational echo of the opioid crisis. Cold Spring Harb Perspect Med 11 (3).
Whittaker, V., 1993. Thirty years of synaptosome research. J. Neurocytol. 22 (9), 735–742.
Whittaker, V., Michaelson, I., Kirkland, R.J.A., 1964. The separation of synaptic vesicles from nerve-ending particles (synaptosomes'). Biochem. J. 90 (2), 293.
Yang, S., Lian, G., 2020. ROS and diseases: role in metabolism and energy supply. Mol. Cell. Biochem. 467, 1–12.
Yazdy, M.M., Desai, R.J., Brogly, S.B., 2015. Prescription opioids in pregnancy and birth outcomes: a review of the literature. J. Pediatr. Genet. 4 (2), 56–70.
Yeoh, S.L., et al., 2019. Cognitive and motor outcomes of children with prenatal opioid exposure: a systematic review and meta-analysis. JAMA Netw. Open 2 (7), e197025-e197025.
Yoshino, A., et al., 1991. Dynamic changes in local cerebral glucose utilization following cerebral concussion in rats: evidence of a hyper-and subsequent hypometabolic state. Brain Res. 561 (1), 106–119.

Zamani, A., Mychasiuk, R., Semple, B.D., 2019. Determinants of social behavior deficits and recovery after pediatric traumatic brain injury. Exp. Neurol. 314, 34–45.
Zhang, Y., et al., 2017. Alterations of expression of inflammation/immune-related genes in the dorsal and ventral striatum of adult C57BL/6J mice following chronic oxycodone self-administration: a RNA sequencing study. Psychopharmacology 234, 2259–2275.
Zhong, Y., et al., 2011. Mitochondrial transcription factor A overexpression and base excision repair deficiency in the inner ear of rats with d-galactose-induced aging. FEBS J. 278 (14), 2500–2510.